

Axion Icebergs: Clockwork ALPs at hadron colliders

Srimoy Bhattacharya,^a Debajyoti Choudhury,^b Suvam Maharana^{c,1} and Tripurari Srivastava^d

^a*School of Physics and Institute for Collider Particle Physics, University of the Witwatersrand, Johannesburg, Wits 2050, South Africa*

^{b,c,d}*Department of Physics and Astrophysics, University of Delhi, Delhi 110007, India*

E-mail: debchou.physics@gmail.com, bhattacharyasrimoy@gmail.com,
smaharana@physics.du.ac.in, tripurarisri022@gmail.com

ABSTRACT: The conventional ultralight QCD axion is typically rendered invisible at collider experiments by its large decay constant. What could also hint at its possible existence is the observation of other (heavy) particles that are characteristically related to the light axion. One such scenario is afforded within the framework of the *clockwork* mechanism where the axion can have suppressed couplings with the gluons or photons while its companion axion-like particles (ALPs) have relatively unsuppressed couplings. We study a minimal clockwork model for the QCD axion invoking a KSVZ-like setup and examine the visibility of the ALPs (a_n) at the LHC through the process $pp \rightarrow a_n$ (+ additional jets), $a_n \rightarrow \gamma\gamma$. The model contains N ALPs with a decay constant f and masses defined by a scale m characteristic of the nearest-neighbour interactions of the scalar fields. For $10 \lesssim m \lesssim 100$ GeV, $f \sim 1$ TeV and $N \sim \mathcal{O}(10)$, the full spectrum of ALPs is accessible and the corresponding diphoton invariant mass distribution comprises a unique signature of a wide band of resonances. For the case of light ALPs ($m \sim \mathcal{O}(10$ GeV)) with the axion being a dark matter candidate, the mass-splittings among the former are so small that the signal profile mimics that of a single broad resonance, or an *axion iceberg*. The effect subsides for heavier ALPs, albeit still exhibiting undulating peaks. For light ALPs, the scenario is imminently testable by the end of LHC's Run 3 phase, with the estimated *cumulative* significance reaching the discovery threshold for an integrated luminosity of ~ 300 fb⁻¹. While the signals for the heavier ALPs in this minimal setup may not be as prominent within the ongoing LHC operation, one could expect to probe a wider parameter space of the model at the forthcoming HL-LHC.

¹Corresponding author

Contents

1	Introduction	1
2	The model	3
2.1	Clockwork scalars	3
2.2	A KSVZ axion	5
2.2.1	The Peccei-Quinn Mechanism	6
2.3	Axion physics above the QCD confinement scale	8
3	Clockwork axions at colliders	9
4	Signal and Background profiles	13
4.1	Light ALPs	13
4.2	Intermediate mass ALPs	17
4.2.1	Benchmark Point II(a)	18
4.2.2	Benchmark Point II(b)	19
4.3	Heavy ALPs	21
5	Vector-like quarks and heavy scalars	24
6	Summary and Conclusion	26
A	The axial anomaly	28
B	VLQ decay widths	29

1 Introduction

The strong CP problem is, perhaps, one of the strongest motivations to look for new dynamics beyond the Standard Model (SM) of particle physics, in particular towards probing the existence of the light pseudoscalar particle predicted by the Peccei-Quinn (PQ) mechanism [1–3] which is, arguably, the simplest and the most elegant solution to the problem proposed to date. The mechanism entails a pseudoscalar field ϕ (popularly called an axion or, more specifically, the QCD axion), that couples to gluons via the interaction term $(\phi/f)\tilde{G}G$. A shift in the field can, then, counter the CP violating topological term $(\theta\tilde{G}G)$ appearing in the SM as a result of the nontrivial structure of the QCD vacuum. There exist interesting alternatives to the PQ scenario as well, most notable among them are solutions based on a massless up quark [4–8] and those invoking spontaneous CP violation (*a la* the Nelson-Barr mechanism) [9, 10]. However, the $m_u = 0$ solution within the standard theory currently stands in tension with the lattice QCD result of the topological mass contribution

[11] and models based on the Nelson-Barr mechanism are also subject to several theoretical challenges [12]. Of course, the axion solution is no less prone to problems of its own. The quality problem and domain wall formation are some of the theoretical and cosmological issues that still plague the mechanism's general viability, although there have been several noteworthy developments towards mitigating these issues [13–16]. Nevertheless, the axion solution offers an interesting, albeit important, domain to explore phenomenologically, more so because the axion can potentially also play the role of an ultralight dark matter candidate [17, 18].

The axion is typically expected to have a very large decay constant ($f \gtrsim \mathcal{O}(10^{10} \text{ GeV})$) depending on its mass so as to be consistent with the current experimental limits on its effective couplings with photons (as also electrons and nucleons) [19, 20]. Furthermore, in the minimal scenarios the QCD axion mass scales inversely with the decay constant and, hence, a large f also implies a very light mass for the axion. The light mass and extremely feeble couplings render the minimal QCD axion nearly invisible to most of the current and future experimental probes. For such scenarios the sensitivities of collider experiments are, understandably, quite poor. Indeed, most current collider searches concentrate, instead, on axion-like particles that either have no role in the strong CP issue [21–23] or have other sources (new or extended confining sectors) which raise their masses substantially [24–29]. This raises the question as to whether the discovery of a massive axion-like particle would necessarily negate the existence of the light QCD axion. We address this by exploring a theoretical scenario wherein the light and nearly invisible QCD axion is naturally accompanied by heavy pseudoscalars having couplings with the gluons and photons large enough to be visible at hadron colliders. One such scenario is realized in the context of a warped 5D (Randall-Sundrum) geometry where the axion field lives in the bulk and the resulting 4D theory contains the invisible axion as the zero mode along with a tower of massive Kaluza-Klein states [30].

In this work, we focus on a relatively new alternative based on the clockwork mechanism which was originally introduced in the context of relaxions [31, 32] and later extended to general field theories [33]. The mechanism primarily entails the generation of hierarchical couplings or mass scales through the localization of the lightest particle in the theory space lattice defined by N fields which interact with each other through nearest-neighbour couplings with a strength characterized by a parameter q . The massive modes, on the other hand, would be delocalized over the entire lattice. With a clockwork theory of $N + 1$ pseudoscalars, then, the zero mode would correspond to the invisible axion with an exponentially large decay constant towards one end of the lattice compared to that of the N delocalized heavy axions in the spectrum. The unsuppressed couplings of the heavy excitations raises the possibility that these may be produced at the LHC in numbers sufficient enough to be detectable. As it turns out, the individual heavy resonance continues to be barely visible over the background. However, their closeness in mass (a consequence of the clockwork paradigm) results in an intriguing signal at the LHC. A similar model has been discussed before in [34], although with the primary focus on enhancing the photon coupling and studying the attendant phenomenology of the light axion, and in [35] in the context of the now obsolete 750 GeV diphoton excess..

The structure of the paper is as follows. In section, 2 we define a minimal clockwork model for a KSVZ-like QCD axion and briefly comment on how it addresses the strong CP problem. In addition to the light QCD axion, the model comprises a characteristic spectrum of massive axion-like particles (ALPs). We identify, in section 3, three benchmark points of the model suitable for probing the ALPs through the gluon-fusion channel at the LHC. In section 4, we discuss the corresponding signal and background profiles for $\sqrt{s} = 13$ TeV and an integrated luminosity $\mathcal{L} = 138 \text{ fb}^{-1}$. Section 5, on the other hand, briefly describes the implications of the vector-like quark and the heavy radial scalars present in the model. Finally, we summarize the results and conclude in section 6.

2 The model

We begin by constructing a clockwork realization of the minimal QCD axion, adopting a KSVZ-like [36, 37] scenario. In the ensuing, we first detail the structure and spectrum of the clockwork sector and then proceed towards describing how the KSVZ setup can be implemented in the context of the clockwork mechanism.

2.1 Clockwork scalars

We define the clockwork (CW) sector in terms of $N + 1$ complex scalars Φ_j , each charged under a global Abelian group $U(1)_j$ described by the Lagrangian

$$\begin{aligned} \mathcal{L}_{\text{CW}} &= \mathcal{L}_1 + \mathcal{L}_2 \\ \mathcal{L}_1 &\equiv \sum_{j=0}^N \left[(\partial_\mu \Phi_j^\dagger)(\partial^\mu \Phi_j) - \lambda \left(\Phi_j^\dagger \Phi_j - f^2 \right)^2 \right], \\ \mathcal{L}_2 &\equiv \lambda' \Lambda^{3-q} \sum_{j=0}^{N-1} \Phi_j^\dagger \Phi_{j+1}^q + \text{h.c.}, \end{aligned} \quad (2.1)$$

where λ, λ' are dimensionless real constants and $\Lambda (\ll f)$ is a characteristic scale associated with \mathcal{L}_2 (the exponent q being, as yet, unspecified). In the absence of \mathcal{L}_2 (*i.e.*, in the limit $\lambda' \rightarrow 0$), the Lagrangian has a $U(1)^{N+1}$ global symmetry, the spontaneous breaking of which, at the scale f (through $\langle \Phi_j^\dagger \Phi_j \rangle = f^2$ for all j) would lead to $(N + 1)$ Goldstone bosons π_j , with the complex scalars being representable as

$$\Phi_j = \frac{1}{\sqrt{2}}(\phi_j + f)e^{i\pi_j/f}, \quad (2.2)$$

where ϕ_j are the corresponding massive scalars. Note that this breaking mechanism still retains the additional global discrete symmetry $\Phi_j \leftrightarrow \Phi_k$ inherent in \mathcal{L}_1 .

The large global symmetry, discrete or continuous (and the attendant plethora of Goldstones in the broken phase) is neither well-motivated nor desirable. Clearly, it can be broken by arbitrary terms expressing interactions between the scalars. On the other hand, at least a single $U(1)$ needs to be present¹ so that its spontaneous breaking could lead to the axion. The interaction Lagrangian \mathcal{L}_2 serves exactly this purpose. Representing perhaps the

¹Understandably, an exact global symmetry is unrealistic because even in the absence of new symmetry breaking effects one would expect the global $U(1)$ to be explicitly broken by quantum gravity effects. The

simplest set of operators which preserve a single $U(1)$ while exhibiting the clockwork mechanism, it can be understood in terms of nearest-neighbour interaction terms² that exhibit locality in a theory space and, hence, the lattice defined by the fields Φ_j (each specifying a *site* in the theory space) can be regarded as the fifth dimension, although a continuum limit of such a construction is difficult to realize. As for the exponent q in \mathcal{L}_2 , a non-integer value would imply compositeness, thereby adding a further layer of complications. The clockwork mechanism, which will be employed in the following discussions, necessitates $q > 1$. On the other hand, for $q > 3$ one would obtain nonrenormalizable operators in \mathcal{L}_{CW} implying that the explicit symmetry breaking takes place due to new dynamics operational at the heavy scale $\Lambda \gg f$ and beyond. This, however, is inconsistent with the notion that $U(1)^{N+1}$ is spontaneously broken at the lower scale f . To avoid such issues and for simplicity we consider a renormalizable theory with $1 < q \leq 3$.

With the introduction of \mathcal{L}_2 , the erstwhile discrete symmetry is completely broken, whereas the $U(1)^{N+1}$ symmetry breaks explicitly to one combination $U(1)_{CW}$ corresponding to the generator,

$$\mathcal{Q}_{CW} = \sum_j \frac{\mathcal{Q}_j}{q^j}, \quad (2.3)$$

with \mathcal{Q}_j being the generators (charges) corresponding to the individual $U(1)_j$'s. Consequently, only one combination of the π_j 's would now be a true Goldstone boson, while all the rest would gain masses much smaller than f . In other words, the latter are now pseudo-Nambu-Goldstone bosons (pNGBs). To be specific, the full scalar Lagrangian, in the broken phase, can be written as,

$$\begin{aligned} \mathcal{L}_{\Phi}^{Full} = & \sum_{j=0}^N \left[\frac{1}{2} \partial_{\mu} \phi_j \partial^{\mu} \phi_j - \frac{1}{4} \lambda (\phi_j + f)^4 \right] \\ & + 2^{(1-q)/2} \lambda' \Lambda^{3-q} \sum_{j=0}^{N-1} (\phi_j + f)(\phi_{j+1} + f)^q \cos \frac{\pi_j - q\pi_{j+1}}{f}. \end{aligned} \quad (2.4)$$

The mass eigenvalues of the pseudoscalar system are given by

$$m_n^2 = \begin{cases} 0 & n = 0 \\ m^2 \left[1 + q^2 - 2q \cos \frac{n\pi}{N+1} \right] & n \neq 0 \end{cases}, \quad (2.5)$$

Planck suppressed symmetry violating terms thus generated can, in general, have serious implications for the QCD axion potential to be discussed later [38]. There are, however, several interesting ways of increasing the degree of Planck suppression, e.g. by considering the scalars to be composites of entities belonging to a new confining sector [39].

²In general, one could also have non-nearest neighbour interactions while keeping the CW symmetry intact, an example being a term of the form $\Phi_j^{\dagger} \Phi_{j+1}^{q/p} \dots \Phi_{j+p}^{q^p/p}$. With reference to eq.(2.5) such a term adds, to the average mass scale of the pNGBs, a contribution $m_a^{(p)} \sim m(q^p/p)$ [40]. For the case $q = 2$ (which would be our primary choice as a benchmark for the collider analysis to be discussed) renormalizability necessitates $p = 1, 2$ for which the overall pNGB mass scale changes only slightly with $m_a \sim \sqrt{2}m_a^{(1)}$. The case for $q = 3$ is a little different with $m_a \sim 3m_a^{(1)}$, although the qualitative aspects of our results and conclusions in this work would be applicable just as well.

where $m^2 \equiv 2^{(1-q)/2} \lambda \Lambda^{3-q} f q^{-1}$ (thus, $m_n^2 \ll f^2$ as was expected). The transformation relation between the unphysical basis (π_j) and the physical basis (a_n) is specified by a matrix C (*viz.* $a_n \equiv \sum_{j=0}^N C_{nj} \pi_j$) with elements

$$C_{0j} = \mathcal{N}_0 q^{-j}, \quad C_{nj} = \mathcal{N}_n \left[q \sin \frac{jn\pi}{N+1} - \sin \frac{(j+1)n\pi}{N+1} \right]. \quad (2.6)$$

Here \mathcal{N}_0 and \mathcal{N}_n are the normalization factors,

$$\mathcal{N}_0 = \sqrt{\frac{q^2 - 1}{q^2 - q^{-2N}}}, \quad \mathcal{N}_{n>0} = \frac{m}{m_n} \sqrt{\frac{2}{N+1}}. \quad (2.7)$$

It is evident from eq.(2.6) that while the heavy pseudoscalars are nearly delocalized over the lattice, the massless mode — which will subsequently assume the role of the QCD axion (a_0) — is localized towards the $j = 0$ site, *i.e.* it has an exponentially suppressed overlap with π_N by virtue of the clockwork mechanism. Interestingly, this feature will eventually ensure that the light axion has a hierarchically large decay constant³ as compared to the heavy axions in the spectrum.

2.2 A KSVZ axion

Now that we have a massless pseudoscalar in the clockwork spectrum, we would like to promote it to the status of a realistic QCD axion. This is most easily carried out by embedding the clockwork sector in any one of the usual QCD axion models. Owing to the singlet nature of the CW scalars the KSVZ construction is the simplest one. To this end, we introduce one generation of Weyl fermions Ψ_L, Ψ_R with the following nontrivial charges under the SM gauge group and the N -th (global) Abelian group⁴ of the CW sector ($G_{SM} \times U(1)_N$),

Field	$SU(3)_c$	$SU(2)_L$	$U(1)_Y$	$U(1)_N$
Φ_N	1	1	0	ξ
Ψ_L	3	1	Y_Ψ	ξ_L
Ψ_R	3	1	Y_Ψ	ξ_R

with the restriction that $\xi = \xi_L - \xi_R$. This is reminiscent of the chiral PQ charges typically assigned to the new (*i.e.*, non-SM) fermions in KSVZ models. The SM fields are assumed to be uncharged under the new $U(1)$'s. For $\xi_L \neq \xi_R$, the new singlet quark cannot have a bare mass term. On the other hand, for the aforementioned choice of $\xi = \xi_L - \xi_R$, the new fermion may now interact with the CW sector through a Yukawa term localized at the N -th site of the lattice. However, with just this interaction, the new quark would be absolutely stable and, hence, phenomenologically untenable. The situation can be remedied only if it couples with the SM fermions which, for our charge assignments, can be most simply

³Note that the usage of the terminology “decay constant” here is different from that encountered in the context of processes such as $\pi^\pm \rightarrow l^\pm \nu$, where π^\pm are the charged QCD pions.

⁴While it is possible to have the $\psi_{L,R}$ charged under all the additional $U(1)$ s, this only adds a layer of complexity without any qualitative changes.

ensured when $\xi_R = 0$ (and, thus, $\xi_L = \xi$) alongwith an appropriate choice of Y_Ψ . To be specific, we choose $Y_\Psi = 2/3$, thereby allowing Ψ to mix with the up-type quarks. The complete set of Yukawa interactions is, thus, given by

$$\mathcal{L}_\Psi \supset -\lambda_\Psi \Phi_N \bar{\Psi}_L \Psi_R - \sum_{\alpha=1}^3 y_\Psi^{(\alpha)} \bar{Q}_L^{(\alpha)} \tilde{H} \Psi_R - \sum_{\alpha=1}^3 y_\Psi^{\prime(\alpha)} \Phi_N \bar{\Psi}_L u_R^{(\alpha)} + \text{h.c.}, \quad (2.8)$$

where $Q_L^{(\alpha)}$ are the SM quark doublets, $u_R^{(\alpha)}$ the up-type singlets and H the SM Higgs doublet. As for the dimensionless couplings λ_Ψ , $y_\Psi^{(\alpha)}$ and $y_\Psi^{\prime(\alpha)}$, the first determines the mass of the Ψ while the other two determine its decay rate. For the sake of simplicity, we assume that $\Psi_{L,R}$ couple to only the third-generation quarks, thereby precluding large flavour-changing neutral currents.

In addition, the CW sector can also couple with the SM Higgs through⁵,

$$\mathcal{L}_{\Phi-H} = -\lambda_{\Phi H} \sum_{j=0}^N \Phi_j^\dagger \Phi_j H^\dagger H \quad (2.9)$$

We will come back to reviewing the dynamics of the heavy radial scalars and the quarks, alongwith the flavour constraints on the Yukawa couplings, in a later section. Alluding to the core objective of the study, we first describe the low-energy physics of the pseudoscalars in the discussions below.

After SSB in the clockwork sector, we have

$$\mathcal{L}_\Psi \supset -\frac{1}{\sqrt{2}} \lambda_\Psi (\phi_N + f) e^{i\xi\pi_N/f} \bar{\Psi}_L \Psi_R - y_\Psi Q_L^{(3)} \tilde{H} \Psi_R - \frac{1}{\sqrt{2}} y_\Psi' (\phi_N + f) e^{i\xi\pi_N/f} \bar{\Psi}_L q_R^{(3)} + \text{h.c.} \quad (2.10)$$

A rephasing of the new fermions with respect to the Goldstone field π_N leads to the following interaction terms with the SM gauge bosons via the chiral anomaly (see appendix A for a discussion)

$$\mathcal{L}_{\pi VV} = -g_{\pi GG} \pi_N G^{A\mu\nu} \tilde{G}_{\mu\nu}^A - g_{\pi BB} \pi_N B^{\mu\nu} \tilde{B}_{\mu\nu}, \quad (2.11)$$

with the coefficients given by

$$|g_{\pi GG}| = \frac{g_s^2}{32\pi^2 f_{\text{eff}}}, \quad |g_{\pi BB}| = \frac{2N_c g'^2 Y_\Psi^2}{32\pi^2 f_{\text{eff}}}, \quad (2.12)$$

and an effective scale defined through $f_{\text{eff}} \equiv f/|\xi|$. Note that while f continues to determine the masses of the Ψ and the Φ_N , it is f_{eff} that encapsulates the pNGB decay constants.

2.2.1 The Peccei-Quinn Mechanism

In order for the light pseudoscalar to be the quintessential QCD axion, it must pose a solution to the strong CP problem. Although ref.[34] already has a brief discussion in this context, we outline here, for completeness, how the clockwork Lagrangian can be consistent with the usual Peccei-Quinn mechanism. The foremost requirement for the mechanism is

⁵For simplicity, we assume uniform value of the coupling $\lambda_{\Phi-H}$ for all j . Relaxing this only adds layers of complications without any qualitative change.

the presence of a global symmetry (atleast an accidental one) in the theory. In our case this symmetry would correspond to the residual clockwork symmetry described in the preceding section (see eq.(2.3)). Now, in eq.(2.11), we can perform a shift in the π_N field so as to exactly cancel the CP violating topological term $-\bar{\theta}(\alpha_S/8\pi)\tilde{G}^{\mu\nu}G_{\mu\nu}$. This, however, is a true cancellation, and a potential solution to the strong CP problem, only when π_N does not acquire a nonzero vacuum expectation value (VEV) after employing the constant shift. It is important to note that the explicit breaking of the $[U(1)]^{N+1}$ symmetry in the clockwork sector, courtesy the nearest-neighbour interactions, does not generate a nonzero VEV for the pseudoscalar fields thanks to the residual shift symmetry $U(1)_{CW}$ [41]. The only other source from where π_N gets a potential is due to nonperturbative effects below the QCD confinement scale. This potential would have the approximate form,

$$V(\pi_N) \sim \Lambda_{QCD}^4 \left[1 - \cos\left(\frac{\pi_N}{f_{\text{eff}}}\right) \right], \quad (2.13)$$

which shows that π_N does not, indeed, acquire a nonzero VEV⁶. Going to the mass basis of the CW axions, the lightest axion, i.e. the KSVZ QCD axion, would then obtain a mass given by [42, 43],

$$m_{a_0} \simeq \frac{f_\pi m_\pi}{f_{\text{eff}} q^N} \frac{\sqrt{m_u m_d}}{(m_u + m_d)}, \quad (2.14)$$

where f_π and m_π are the pion decay constant and mass, respectively, and $m_{u,d}$ are the masses of the light SM quarks u and d . Clearly, the light axion has a mass that is exponentially suppressed by the factor q^N as a result of the clockwork localization. Consequently, one need not assume a very large scale f in this scenario to accommodate a QCD axion. For example, with $q = 2$ and $N \gtrsim 15$ one obtains sub-eV masses for the a_0 even for $f \lesssim 1$ TeV (equivalently, f_{eff} in the few hundred GeVs range). From eq.(2.11), it is apparent that such an additional suppression also appears in the axion's coupling with gluons and the electroweak bosons above the confinement scale in the form of the effective decay constant $f_0 = q^N f_{\text{eff}}$. Therefore, with a nominal choice of values for the CW parameters q and N , and a PQ-esque scale f_{eff} which is not too far from the EW scale, we can have a viable QCD axion that is well within the current experimental bounds on f_0 with respect to the light axion mass [20, 44]. These constraints are summarised in Fig.1 where the yellow line reflects the mass vs f_0 relation as given in eq.(2.14) for a QCD axion. The plot shows limits from various EDM experiments [45–47] as well as atomic and molecular transition experiments [48, 49]. On the other hand, the observational limits shown include those obtained from axion star decays (assuming post-inflationary SSB and axion star formation) [50], BBN (constraining axion DM) [51], black hole spins [52–54], pulsars and solar core [55], binary neutron star gravitational wave [56], CMB (Planck) and baryon acoustic oscillation (BAO) [57], SN1987a [58] and white dwarfs [59].

It is perhaps useful to remark here that the potential in eq.(2.13) is a special case which defines a unique vacuum with a domain wall number $N_{DW} = 1$. This is a direct

⁶Naively, the potential would have a degenerate set of minima at $\langle \pi_N \rangle = 2n\pi f_{\text{eff}}$ for integral values of n . However, such nonzero VEVs are unphysical as they can always be shifted to zero by the residual symmetry transformation $\pi_N \rightarrow \pi_N + 2n\pi f_{\text{eff}}$ as a result of the 2π periodicity of the potential.

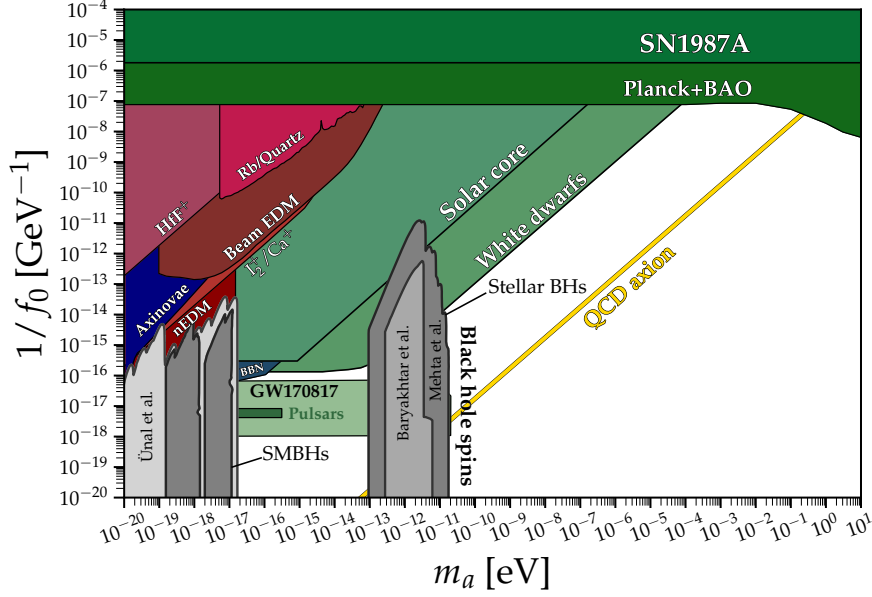


Figure 1: Limits on the effective decay constant f_0 of the light QCD axion vs its mass. Plot adapted from ref.[20].

consequence of the fact that we have invoked only a single generation of the extra $SU(2)$ singlet coloured fermion Ψ . Similar to the $N_{DW} > 1$ scenarios, cosmological domain walls would also form in this case at temperatures near the QCD phase transition scale, albeit with a simple structure where each wall is bounded by an individual cosmic string. Such a simple string-wall network, however, is highly unstable and would be prone to a rapid collapse [60–62]. Thus, apart from the obvious simplicity, the choice of a single species of the singlet heavy quark possesses the important feature of alleviating the domain wall problem [63] typical to axion models.

2.3 Axion physics above the QCD confinement scale

Concerned with the physics observable at high energy colliders, it suffices to consider the theory at energy scales below the EW symmetry breaking scale but significantly above the QCD confinement scale. At these scales, the axion Lagrangian becomes

$$\mathcal{L}_{\pi vv} = -g_{\pi gg} \pi_N G^{A\mu\nu} \tilde{G}_{\mu\nu}^A - g_{\pi\gamma\gamma} \pi_N F^{\mu\nu} \tilde{F}_{\mu\nu} - g_{\pi\gamma Z} \pi_N F^{\mu\nu} \tilde{Z}_{\mu\nu} - g_{\pi ZZ} \pi_N Z^{\mu\nu} \tilde{Z}_{\mu\nu}. \quad (2.15)$$

The coefficients in this case are given by,

$$\begin{aligned} g_{\pi gg} &= \frac{\alpha_s}{8\pi f_{\text{eff}}}, & g_{\pi\gamma\gamma} &= \frac{2N_c \alpha_{EM} Y_\Psi^2}{8\pi f_{\text{eff}}}, \\ g_{\pi\gamma Z} &= \frac{-4N_c s_w^2 \alpha_{EM} Y_\Psi^2}{8\pi f_{\text{eff}} s_w c_w}, & g_{\pi ZZ} &= \frac{2N_c s_w^4 \alpha_{EM} Y_\Psi^2}{8\pi f_{\text{eff}} s_w^2 c_w^2}. \end{aligned} \quad (2.16)$$

where $s_w \equiv \sin \theta_w$ and $c_w \equiv \cos \theta_w$ with θ_w being the Weinberg angle. The effective couplings of the physical axions are then readily obtained using eq.(2.6),

$$\begin{aligned} |g_{agg}^{(n)}| &= \frac{\alpha_s}{8\pi f_n}, & |g_{\pi\gamma\gamma}^{(n)}| &= \frac{2N_c\alpha_{EM}Y_\Psi^2}{8\pi f_n}, \\ |g_{a\gamma Z}^{(n)}| &= \frac{4N_c s_w^2 \alpha_{EM} Y_\Psi^2}{8\pi f_n s_w c_w}, & |g_{\pi ZZ}^{(n)}| &= \frac{2N_c s_w^4 \alpha_{EM} Y_\Psi^2}{8\pi f_n s_w^2 c_w^2} \end{aligned} \quad (2.17)$$

where $f_n \equiv f_{\text{eff}}/|C_{nN}|$ denotes the effective decay constant of the n -th physical axion. It is then readily apparent that the decay constants of the heavy pseudoscalars are hierarchically smaller than that of the light axion. For a SSB scale $f \sim \mathcal{O}(\text{TeV})$, this engenders significantly enhanced couplings of the heavy axions with gluons and the electroweak bosons as compared with those associated with typical light ALP candidates. This enhancement, in principle, can facilitate resonant production of the heavy CW axions at hadron colliders, which is going to be the main subject of discussion in the ensuing sections.

3 Clockwork axions at colliders

As is already described above, the (light) axion, when compatible with the constraints from astrophysical and low-energy experiments [64], is nearly invisible at high energy collider experiments. What seems promising, instead, is the prospect of probing the heavy pseudoscalars (hereafter, also referred to as axion-like-particles or ALPs) at the LHC and its forthcoming high-luminosity upgrade (HL-LHC). In this case, the production would be dominated by the gluon fusion channel with the hadronic cross-section given by

$$\hat{\sigma}(pp \rightarrow a_n) = K_\sigma^0 \frac{d\mathcal{L}_{gg}}{d\hat{s}} \bigg|_{\hat{s}=m_n^2} \frac{\pi^2}{8m_n} \Gamma_{gg}^{(n)} \delta(\hat{s} - m_n^2), \quad (3.1)$$

where $d\mathcal{L}_{gg}/d\hat{s}$ is the gluon-gluon luminosity and the K -factor K_σ^0 encapsulates the higher order QCD corrections. Using the MSTW2008nn1o68 parton densities, ref.[65] estimates $K_\sigma^0 \approx 3.7$. (including the full NNLO and approximate N³LO corrections [66–69]) over the pseudoscalar mass range 40 – 125 GeV. In the absence of a full computation of the QCD corrections, we make the reasonable extrapolation that $K_\sigma^0 \sim 3.7$ for the mass range 10–125 GeV. For ALP masses beyond 150 GeV we assume a more conservative $K_\sigma^0 = 2.5$ [69].

The leading (two-body) decay channels and the corresponding widths for the ALPs are

$$\begin{aligned} \Gamma(a_n \rightarrow gg) &\equiv \Gamma_{gg}^{(n)} = K_{gg} C_{n,N}^2 |g(x_n)|^2 \frac{\alpha_S^2}{32\pi^3} \frac{m_n^3}{f_{\text{eff}}^2} \\ \Gamma(a_n \rightarrow \gamma\gamma) &\equiv \Gamma_{\gamma\gamma}^{(n)} = 9Y_\Psi^4 C_{n,N}^2 |g(x_n)|^2 \frac{\alpha_{EM}^2}{64\pi^3} \frac{m_n^3}{f_{\text{eff}}^2} \\ \Gamma(a_n \rightarrow Z\gamma) &\equiv \Gamma_{Z\gamma}^{(n)} = 9Y_\Psi^4 C_{n,N}^2 |g(x_n)|^2 \frac{\alpha_{EM}^2 \tan^2 \theta_w}{8\pi^3} \frac{(m_n^2 - m_Z^2)^3}{m_n^3 f_{\text{eff}}^2} \\ \Gamma(a_n \rightarrow ZZ) &\equiv \Gamma_{ZZ}^{(n)} = 9Y_\Psi^4 C_{n,N}^2 |g(x_n)|^2 \frac{\alpha_{EM}^2 \tan^4 \theta_w}{64\pi^3} \frac{(m_n^2 - 4m_Z^2)^{3/2}}{f_{\text{eff}}^2} \end{aligned} \quad , \quad (3.2)$$

where $x_n \equiv 4m_\Psi^2/m_n^2$ and the loop-integral $g(x)$ is defined as,

$$g(x) \equiv \begin{cases} x \left[\sin^{-1}(x^{-1/2}) \right]^2 & x \geq 1 \\ \frac{-x}{4} \left[\ln \frac{1 + \sqrt{1-x}}{1 - \sqrt{1-x}} - i\pi \right]^2 & x < 1. \end{cases} \quad (3.3)$$

In the expression for Γ_{gg} , the QCD correction amounts to $K_{gg} = 2.1$ [70]. Clearly, the ALPs decay dominantly to two gluons followed by decays to photons (and to $Z\gamma$ and ZZ depending on kinematic feasibility). It is easy to infer in the narrow width approximation that the dijet cross-section would exceed the diphoton one by a factor of $[2/(9Y_\Psi^4)]K_{gg}(\alpha_S^2/\alpha_{EM}^2)$. However, as far as detection at hadron colliders is concerned, the diphoton final state, understandably, offers better sensitivity as compared to the dijet channel. We will, therefore, consider only the processes $pp \rightarrow a_n \rightarrow \gamma\gamma$ for the case in hand.

The diphoton final state has been extensively studied in the literature in the context of spin-0 and spin-2 resonances, with dedicated searches from the ATLAS and CMS collaborations spanning almost the entire range of masses accessible with current sensitivities. With no discernible excess of events over the SM background reported thus far, the most recent analyses from ATLAS [71–73] and CMS [74, 75] place the strongest limits to date on the $pp \rightarrow \gamma\gamma$ fiducial cross-section for spin-0 resonances over a wide mass bracket ranging from nearly 10 GeV to a few TeVs. Being optimistic that some new physics indeed exists beyond the SM, this broadly implies two possibilities — one, that the energy scale of new physics lies beyond the reach of the LHC and, two, that new dynamics exist within the LHC’s energy reach, albeit with feeble interaction strengths with the SM so as to be inaccessible with the current luminosity reach. In the following, we choose the latter viewpoint and explore viable scenarios where the diphoton cross-sections for the CW pseudoscalar spectrum could be very close to the current exclusion limits at the LHC obtained from the Run-2 data, such that a sizable enhancement in the signal significance can be achieved by the end of the ongoing Run-3 phase. This is interesting because even if a 5σ discovery looks improbable at the LHC, such enhancements could hint at a potential discovery at the HL-LHC taking into account the projected integrated luminosity of $\sim 3000 \text{ fb}^{-1}$, *i.e.* nearly 20 times the luminosity achieved by the end of LHC Run-2 ($\sim 138 \text{ fb}^{-1}$). We consider for our study three benchmark points categorized by the ALP masses in the range 10 – 30 GeV, 35 – 105 GeV (with two sub-categories in this case) and 150 – 450 GeV, respectively, and have as guiding references the ATLAS analyses carried out in [71–73].

For each of the benchmark points, we choose $\xi = 3$ and $q = 2$ (as the middle point of the theoretically allowed range) and also assume $Y_\Psi = 2/3$ so that the Ψ may mix with the top quark. The other particulars are as follows—

Benchmark I: We assume the parameter values $N = 28$, $m = 10$ GeV and $f = 1000$ GeV in the CW sector. The resulting light axion mass in this case is $m_{a_0} \sim 6.4 \times 10^{-5}$ eV and the ALP masses span the range ~ 10 –30 GeV. This particular choice of the CW parameters, especially the sizable number of particles N , is also motivated by the fact that this allows for the light axion to be a DM candidate [76]. With these choices in place, we can determine the diphoton cross-section in the narrow-width approximation (NWA). Fig.2a shows the cross-

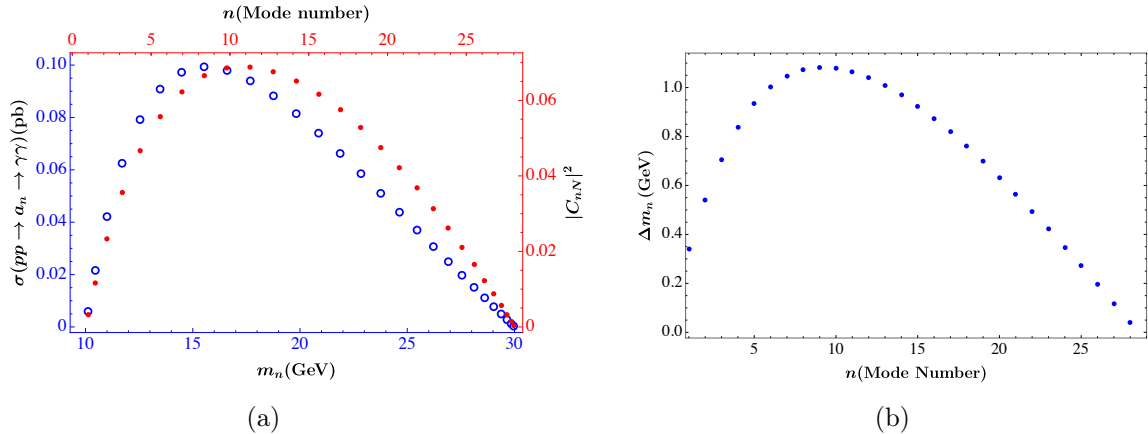


Figure 2: (a) Masses and couplings for individual ALPs and corresponding diphoton cross-sections for benchmark I. The vertical axis on the right shows the extent of the field π_N contained in the mass eigenstates a_n . (b) Mass-splittings between consecutive ALPs for benchmark I.

sections for each of the ALPs (integrated over the full final state phase-space) computed for a center of mass energy $\sqrt{s} = 13$ TeV using the NNPDF2.3L0 PDF set [77]. Note that the cross-section peaks for an intermediate mode of the spectrum, the exact identity of which depends on the periodic variation of the couplings due to the clockwork mixing as well as the energy dependence of the parton-parton luminosity. Fig.2b, on the other hand, shows Δm_n (the mass-splitting between consecutive CW modes) along the full spectrum, with the average mass-splitting being given by $\Delta m \sim 2m/N$. It is interesting to note that, with the consecutive differences $\Delta m_n \lesssim 1$ GeV over the entire extent of the ALP spectrum, the splittings are comparable with the prevailing detector resolution. Consequently, the individual resonances may not be entirely resolved and the events corresponding to the full spectrum (subject to the assumed bin size) may even appear as a single broad resonance⁷ within an envelope of mass width $\sim \Delta m$ in the diphoton invariant mass distribution.

Benchmark II: (a) The parameter configuration in the CW sector for this case is — $m = 35$ GeV, $N = 28$ and $f = 1000$ GeV. The light axion mass remains the same as in benchmark I while the ALP masses now range from 35 to 105 GeV. The corresponding diphoton cross-sections are shown in Fig.3a. Due to an increase in the value of the parameter m (by a factor of 3.5) the mass-splittings in this case, readily inferred from eq.(2.5), are nearly triple in value compared to that in the preceding case. Therefore, in stark contrast with benchmark I, one expects to discern at least a few individual peaks in the invariant mass distribution of the signal events. We will see that this is indeed the case.

(b) Now, eschewing the notion of a_0 as a DM candidate, we assume a larger set of CW scalars, namely $N = 40$, while keeping the rest of the parameters the same as in II(a). Then, from eq.(2.14) it is clear that the light axion mass lowers to a value $m_{a_0} \sim 1.5 \times 10^{-8}$ eV. The mass splittings in this case fall in the range $\sim 0.5 - 2.7$ GeV — smaller than what

⁷This was also hinted at in ref.[35].

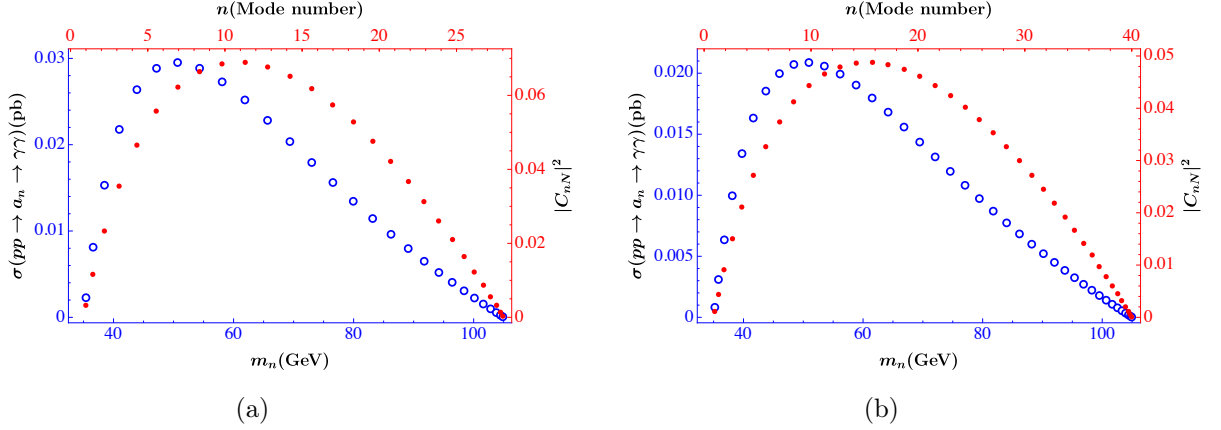


Figure 3: Masses and couplings for individual ALPs and corresponding diphoton cross-sections. (Left) benchmark II(a) and (right) benchmark II(b).

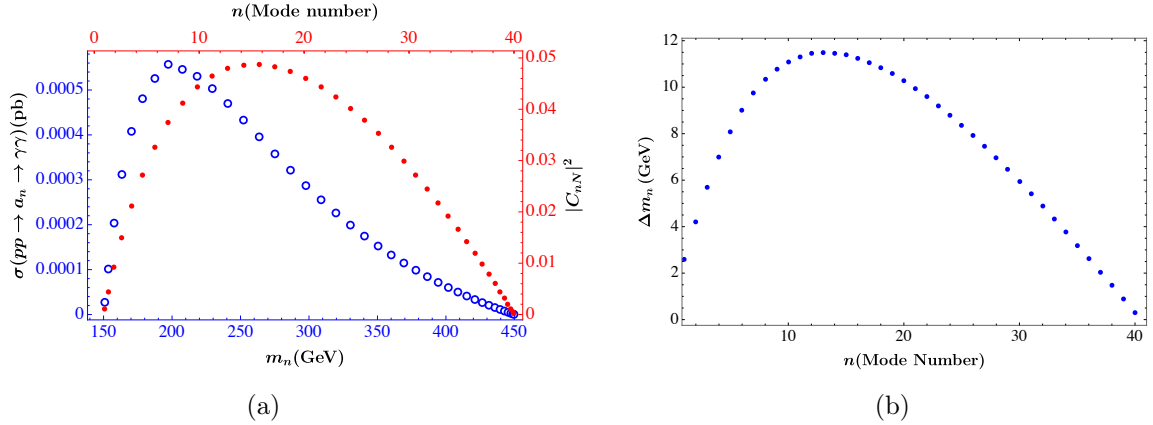


Figure 4: Diphoton cross-sections and mass-splittings for benchmark III.

we obtained in benchmark II(a) but not small enough to be completely unresolved at the detector. Consequently, the distribution of signal events, as a function of the diphoton invariant mass is expected to be an undulating one.

Benchmark III: Exploring ALPs heavier than the SM Higgs, we consider $m = 150$ GeV, $N = 40$ and $f = 1600$ GeV. Due to the increase in the SSB scale f , the QCD axion mass is now even slightly lower than that in benchmark II(b), namely $m_{a_0} \approx 9.7 \times 10^{-9}$ eV. As before, Fig.4 shows the diphoton cross-sections for the ALP spectrum as well as the characteristic mass-splittings.

With the model parameters defined, we now simulate the diphoton signal events and compare with the corresponding SM backgrounds for the 13 TeV LHC. We write the Feynman rules of the models in `Feynrules` [78] and generate UFO files that are then imported in the `MadGraph5` [79] event generator for a Monte Carlo simulation of the signal. Further, `Pythia8` [80, 81] is used for parton showering and hadronization. Final state objects at the detector level are reconstructed using the fast simulation tool `Delphes` [82]. Within

Delphes we choose to simulate the detector effects using the ATLAS detector card for the entirety our study.

The SM diphoton (with and without jets) background at the LHC has been very well-studied by both the ATLAS and CMS collaborations, not only in the context of the SM Higgs, but also for other exotic resonances, light and heavy. Indeed, there have been occasional reports of excesses, only to largely vanish on account of an even more careful recalibration of the backgrounds. We would be largely using the ATLAS analyses to estimate the backgrounds and, by extension, use the same kinematical restrictions *etc.* to estimate the signal strength as well.

4 Signal and Background profiles

While we would be concentrating on ALPs being produced in gluon fusion and decaying into a diphoton pair, note that the exact final state would be dependent on the average mass of the ALPs. In particular, a very light ALP, produced sans any accompanying high- p_T particle, would result in a pair of relatively soft photons that would, typically, fail trigger requirements. In other words, a minimal number of high- p_T entities must be present, and thus, both signal and background estimations would need to be done accordingly.

4.1 Light ALPs

For **Benchmark Point I**, the ALP masses are in the 10 – 30 GeV range, and the final state photons need to be boosted to overcome the detector’s trigger level energy threshold. To achieve this, we follow the strategy employed in the ATLAS search [71] (and also ref.[65]) for low mass diphoton resonances and consider a diphoton final state with upto two additional jets. To simulate the signal events we first generate⁸ $pp \rightarrow a_n + 0/1/2$ partons at the leading order (LO), using **MadGraph5**, for $\sqrt{s} = 13$ TeV with the NNPDF2.3LO PDF set, followed by the two-body decay of the on-shell ALPs⁹. This is followed by parton showering and hadronization via **Pythia8** [80, 81]. Matching and merging of the matrix elements (including the avoidance of overcounting) for showering is automated using the MLM matching scheme.

As mentioned previously, for a detector level simulation of the showered events we use the **Delphes** tool. The following summarizes the criteria used to identify and isolate final state objects.

Jets: Within **Delphes**, jets are reconstructed using the **FastJet** package [84]. Jet clustering is performed using the anti- k_T algorithm [85] with the jet cone radius parameter R chosen to be 0.4. To be consonant with the ATLAS analyses, we require the minimum transverse momentum of jets p_{Tj} to be 20 GeV and its pseudorapidity to satisfy $|\eta_j| < 2.5$. Finally, any two jets must be separated by $\Delta R(j, j) > 0.7$ where $(\Delta R) \equiv [(\Delta\eta)^2 + (\Delta\phi)^2]^{1/2}$ is the separation in the pseudorapidity-azimuthal angle plane.

⁸Understandably, this is overwhelmingly dominated by the subprocesses wherein the final state partons are gluons.

⁹Given that the ALPs are spinless, there are no non-trivial spin correlations. Furthermore, given that they are very narrow, there is no real loss of information or accuracy in the neglect of possible off-shell effects, as can also be confirmed by the use of tools such as the **Madspin** [83] module.

Photons: For identification and isolation of photons, a cone size of $\Delta R = 0.2$ around the photon candidate is considered. Denoting the ratio of the sum of transverse momenta of isolated objects (tracks, calorimeter towers, etc) to the candidate’s transverse momentum as p_T^{ratio} , it is demanded that $p_T^{\text{ratio}} < 0.05$. Also incorporated is a p_T -dependent photon identification efficiency (following the ATLAS analysis of ref.[71]) that ranges from $\approx 70\%$ at $p_T = 22$ GeV to $\approx 90\%$ for $p_T > 50$ GeV.

In addition, we ensure angular separation between photons or jets by demanding that $\Delta R(\gamma, \gamma) > 0.2$ and $\Delta R(\gamma, j) > 0.4$. Finally we demand events with at least two photons and at least a jet in the final state by imposing $N_\gamma \geq 2$ and $N_j \geq 1$. The above conditions are summarised in Table 1 for quick reference.

Channel	Acceptance Cuts
$pp \rightarrow a_n + 0/1/2$ jets $a_n \rightarrow \gamma\gamma$	<u>Photon identification</u>
	$\Delta R = 0.2, p_T > 0.5$ GeV, $p_T^{\text{ratio}}(\gamma) < 0.05$
	<u>Jet identification</u>
	$\Delta R = 0.4$ (anti- k_T), $p_T^j > 20$ GeV, $ \eta_j < 2.5$
	<u>Isolation</u>
	$\Delta R(\gamma, \gamma) > 0.2, \Delta R(\gamma, j) > 0.4, \Delta R(j, j) > 0.7$
	$N_\gamma \geq 2, N_j \geq 1$

Table 1: Acceptance cuts for the final state objects in benchmarks I and II [71].

As for the QCD corrections to the process, within the narrow width approximation, we may factorise these separately for the production and the subsequent decay. For such masses of the ALPs, the QCD corrections to the production cross section can largely be summarised in terms of K -factors, with $K_\sigma^1 \sim K_\sigma^2 \simeq 2$ [86] where the superscript indicates the number of jets in the final state. As for the decay, while the correction to the photonic branching fraction is small, that to the gluonic one is substantial, *viz.* $K_{gg} = 2.1$ [70], and serves to scale the diphoton branching fraction (since $\text{BR}_{\gamma\gamma} \approx \Gamma_{\gamma\gamma}/\Gamma_{gg}$). For the effective K -factor, then, $K_\sigma^{1,2}/K_{gg} \approx 1$ for the two benchmark points with light ALPs.

Using `MadAnalysis5` [87] to analyze the signal events following the acceptance cuts, we order the photons and the jets (wherever applicable) in terms of their p_T and present, in Fig.5 (left), the corresponding distributions, for an integrated luminosity of $\mathcal{L} = 138 \text{ fb}^{-1}$. In this, we use a bin size of 1 GeV, as in the ATLAS analysis [71]. While the sharp edges (at 20 GeV) in the jet p_T ¹⁰ distributions are but reflections of the acceptance cut imposed, the fast fall off at higher p_T s is characteristic of QCD radiation. The positions of the peaks are just caused by an interplay of the two effects. As for the photons, the decay of an ALP, in its rest-frame, is isotropic with each daughter photon having an energy equalling half the ALP mass. This distribution, of course, has to be convoluted with the p_T of the ALP itself (as counterbalancing the jet p_T s). And, finally, there are additional convolutions with both the ALP mass-spectrum and the corresponding production cross sections.

¹⁰Note that the events with 2 jets are only a subset of the accepted set of events.

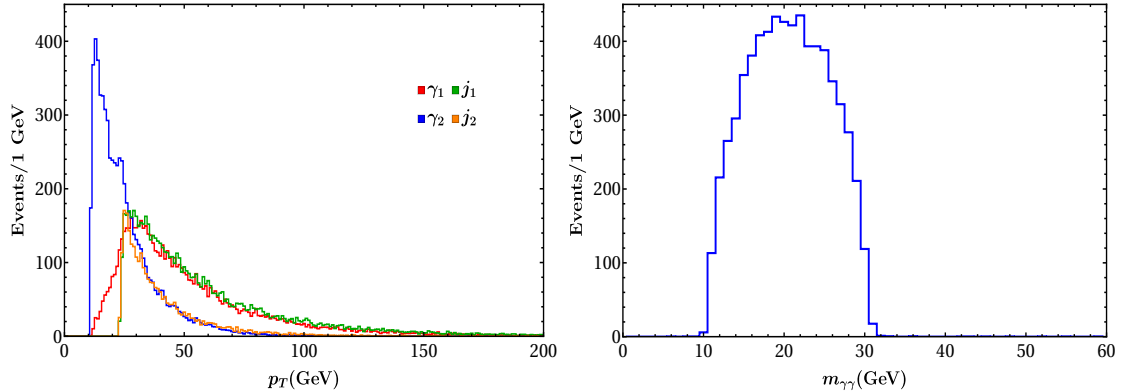


Figure 5: BP-I: event distributions, after applying acceptance cuts alone, *vide.* Table 1. **(left)** p_T distributions for the leading photon (γ_1), sub-leading photon (γ_2), leading jet (j_1) and the sub-leading jet (j_2) and **(right)** the two-photon invariant mass.

Of particular interest is the diphoton invariant mass distribution (Fig.5 (right)) which encompasses the contributions of the entire spectrum of the 28 ALPs. It is instructive to note the difference with the total production cross section (as in Fig.2a) which shows a maximum for $m_a \approx 15$ GeV, owing, as we have discussed, to a combination of the variation in the coupling strength as well as the gluon-gluon flux. However, once the extra jets are required to be radiated, the kinematics (and the mass-dependence of the flux) does change considerably. Even more importantly, the requirements¹¹ on $p_T(\gamma)$ serve to suppress the contribution from the very low mass ALPs, resulting in the significantly shifted maximum (now around $m_{\gamma\gamma} \approx 20$ GeV) as in Fig.5 (right).

For the background, diphoton (associated with additional jets) initiated by $q\bar{q}$ - as well as gg - within SM are considered. However, since there is a finite probability for a putative jet masquerading as a photon in the detector (this is especially true of a low energy jet depositing a large fraction of its energy in the electromagnetic calorimeter), one needs to consider such contributions as well. Thus, the backgrounds emanate primarily from

- $pp \rightarrow \gamma\gamma$,
- $pp \rightarrow \gamma j$,
- $pp \rightarrow jj$.

in each case, accompanied by upto two additional jets.

Other backgrounds emanate from e^\pm not leaving discernible tracks, thereby faking photons. These, though, contribute negligibly and can, therefore, be ignored. For an estimate of the relevant background distribution in the diphoton spectra we again refer to the ATLAS analysis [71] wherein the fiducial region in the phase-space is defined using the

¹¹Further corrections arise from the p_T -dependence of the detector efficiencies.

selection cuts on E_T^γ , $p_T^{\gamma\gamma}$ and η_γ as mentioned in Table 2. The diphoton background¹² thus determined in the analysis has an uncertainty which is predominantly statistical.

Channel	Event Selection Criteria
$pp \rightarrow a_n + 0/1/2 \text{ jets}$ $a_n \rightarrow \gamma\gamma$	$N_\gamma = 2, 1 \leq N_j \leq 2,$ $ \eta_\gamma < 2.37$ (excluding barrel-to-endcap region $1.37 < \eta_\gamma < 1.52$), $E_T(\gamma) > 22 \text{ GeV}, p_T^{\gamma\gamma} > 50 \text{ GeV}$

Table 2: Selection cuts applied to form the fiducial signal regions for benchmarks I and II [71].

To examine the viability of the diphoton signal in the light of the ATLAS analysis, we must subject the former to the same selection criteria as the latter. These are listed in Table 2. As an examination of Fig.5 (left) shows, the $E_T(\gamma)$ cut, especially when applied to the subleading photon, does eliminate a non-negligible fraction of the signal events. Even harder is the cut on $p_T(\gamma\gamma)$, for this requires that the ALP (and, hence, the radiated off jets) must carry a substantial p_T . The consequent reduction of events is reflected in the $m_{\gamma\gamma}$ distribution as shown in Fig.6.

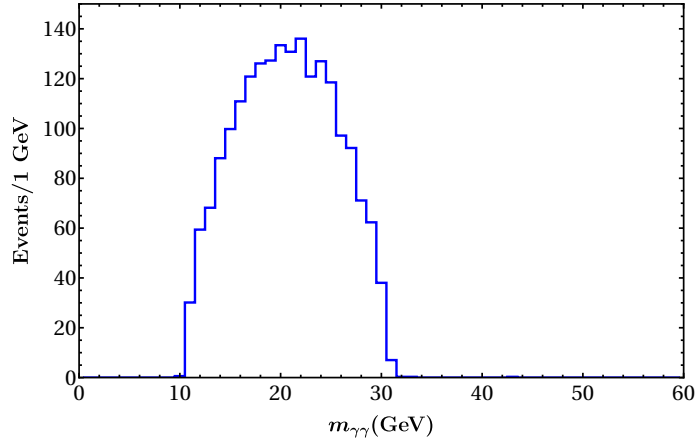


Figure 6: BP-I: Diphoton invariant mass distribution after applying selection cuts.

A striking aspect to note here (this was already evident in Fig.5 (right)) is that although the diphoton distribution receives contributions from all the ALPs in the spectrum, the separation between the individual resonances is smeared by the detector resolution¹³ to a degree that the entire distribution appears as a single broad resonance — an *iceberg* of axions, so to say — with a FWHM $\sim 16 \text{ GeV}$. This feature, as previously mentioned, is peculiar to the clockwork spectrum for any mass scale m as long as N is adequately large.

¹²The background distribution as estimated in the ATLAS analysis [71] for a bin size of 1 GeV is available at <https://atlas.web.cern.ch/Atlas/GROUPS/PHYSICS/PAPERS/HIGG-2019-23/>.

¹³We have made use of the energy resolution function for the ATLAS detector’s ECAL [88] as implemented within *Delphes*. For the phase-space region of interest throughout the presented analysis (i.e. for BP-I, II and III), the energy resolution of the individual photons varies roughly in the range $\sim [0.32, 2.3] \text{ GeV}$.

We can now estimate the significance of the signal events over the background bin-by-bin using $S = N_{sig}/\sqrt{N_{sig} + N_{bkg}}$, where N_{sig} and N_{bkg} denote the number of signal and background events, respectively, in a particular bin. Since the background uncertainty is statistics dominated, this gives quite a robust estimate of the sensitivity and can be bettered only by a dedicated search. The bin-wise significances (and the corresponding p -values) are depicted in Fig.7, and the maximum individual significance of $S_{138}^{1\text{GeV}} \sim 1\sigma$ is obtained in the bin corresponding to $m_{\gamma\gamma} \sim 21 - 22$ GeV. It is tempting to increase the bin widths as this would be expected to substantially increase the per-bin significance owing to the individual peaks being closely packed within the invariant mass range $10 - 30$ GeV. However, since the existence of a wide band of resonances is characteristic to the clockwork scenario, the shape of the invariant mass distribution could itself behave as a discriminator— more so in the case of small mass-splittings— and by enlarging the bin width one would, obviously, lose information about the underlying profile of the spectrum. In particular, this would help discriminate between a broad resonance and multiple sharp ones¹⁴. A more useful method of estimating the total signal significance would be to consider the sum $\sum_i S_i^2$ which, of course, is χ^2 -distributed for the appropriate degrees of freedom. Using this, we find for this benchmark point, the expected cumulative significance to be $S_{c,138} = 3.38\sigma$ for $\mathcal{L} = 138\text{fb}^{-1}$. On the same note, it is worth alluding to the prospect that the significance can further build up by a sizable amount with an increase in the luminosity, even by as early as the end of the ongoing Run-3 phase of the LHC with a projected luminosity reach of $\sim 300\text{fb}^{-1}$. A simple estimate of this can be obtained by scaling the current significance with the luminosity, i.e.

$$S_{c,300} = S_{c,138} \times \sqrt{\frac{300}{138}} \approx 4.98\sigma, \quad (4.1)$$

which makes this benchmark point imminently testable by the end of Run 3.

Apropos of the current benchmark point, Fig.8 shows the variation of S_c with the SSB scale f for the 138fb^{-1} luminosity case alongwith a projection for the 300fb^{-1} reach of the LHC. The variation follows the relation $S_c \propto f^{-2}$ which can be understood from the fact that for a particular choice of the CW parameters the pertinent cross-sections scale roughly as f^{-2} with the pole masses being quite insensitive to it.

4.2 Intermediate mass ALPs

With an intermediate mass range set by the parameters $m = 35$ GeV and $f = 1000$ GeV, the analysis particulars in this case are largely the same as described for benchmark I. With the ALP masses in this case spanning the range $35 - 105$ GeV, a sizable fraction of the spectrum still falls in the low mass region for which we require the final state photons to be boosted due to reasons delineated for benchmark I. We, therefore, choose to adopt the same strategy as in benchmark I for the collider simulation and consider a signal consisting of CW axions produced in association with upto two jets (and the axions further decaying

¹⁴A further discriminant here would be the comparison between the width of the resonance and the total signal size. For a resonance, production cross section is simply related to the total width, whereas the size of the signal is just the product of the cross section, the branching fraction and the overall detector efficiency (the last being a known quantity).

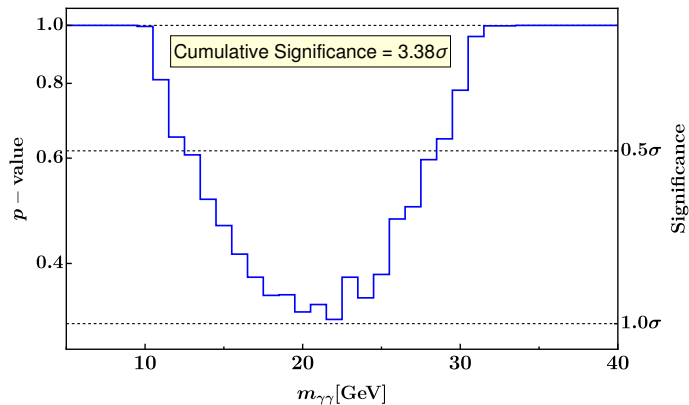


Figure 7: Bin-wise significance for benchmark I at the LHC for $\mathcal{L} = 138 \text{ fb}^{-1}$.

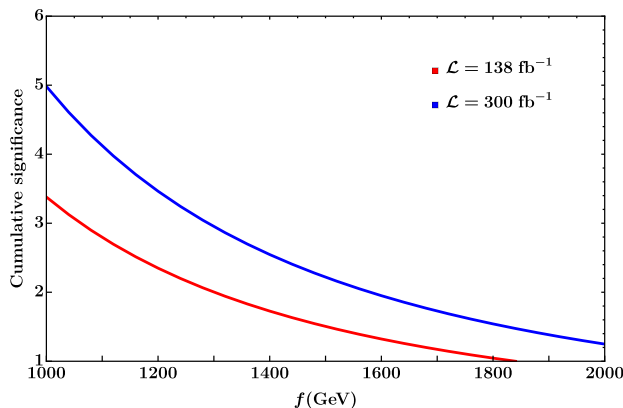


Figure 8: Cumulative significance as a function of the SSB scale f for benchmark-I at the Run 2 (red curve) and Run 3 LHC (blue curve).

to two photons). Photons and jets are reconstructed using the same criteria as in the case of Benchmark point I (see Table 1).

4.2.1 Benchmark Point II(a)

The p_T distributions for the leading and the sub-leading photons thus obtained for the signal events along with the corresponding distributions for the jet p_T 's are shown in Fig.9 (left), assuming a bin size of 1 GeV. The distributions are similar in nature to what was obtained for benchmark point I, albeit with a shift in the photon distributions towards higher p_T values due to the ALPs being heavier in this case. The attendant diphoton invariant mass distribution is shown in Fig.9 (right). As for the SM backgrounds, for the mass range $m_{\gamma\gamma} \in [10, 80]$ GeV, once again we adopt the ATLAS analysis [71]. For the $[80, 110]$ GeV window, in the absence of an appropriate analysis¹⁵, we choose to *overestimate*

¹⁵The ATLAS search for diphoton resonances in the mass range $m_{\gamma\gamma} = 66 - 110$ GeV [89] does provide a background estimation in the region of interest. However, the event selection criteria employed therein is different than that in the low mass analysis that we refer to, which makes it difficult to match the background events corresponding to the low and intermediate mass ranges in a meaningful way.

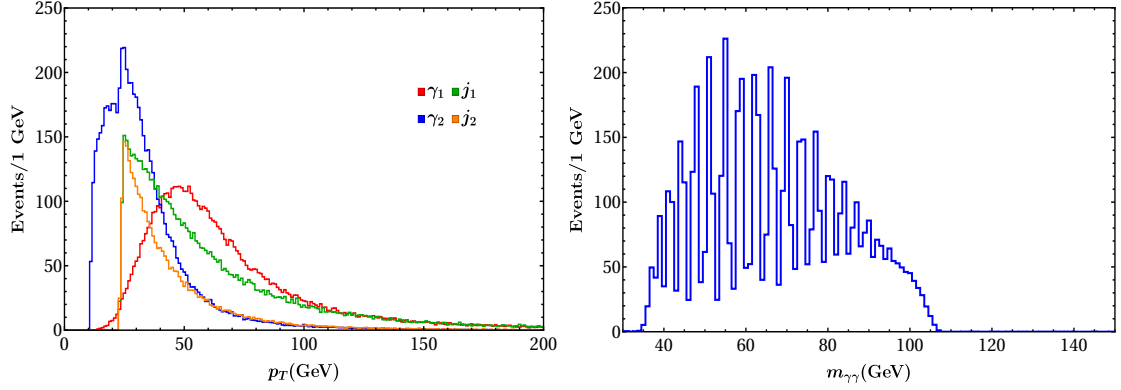


Figure 9: BP-II(a): event distributions, after applying acceptance cuts alone, *vide* Table 1. **(left)** p_T distributions for the leading photon (γ_1), sub-leading photon (γ_2), leading jet (j_1) and the sub-leading jet (j_2) and **(right)** the two-photon invariant mass.

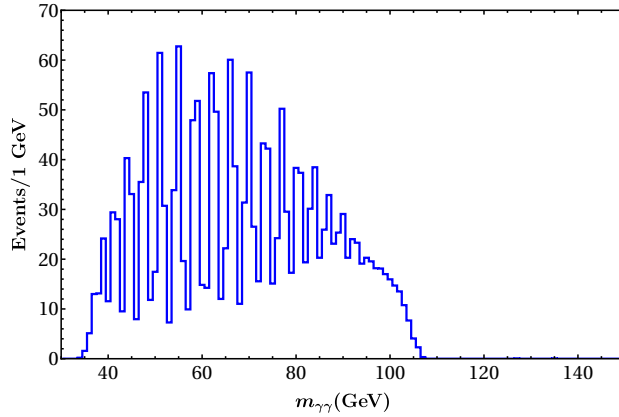


Figure 10: BP-II(a): Diphoton invariant mass distribution after applying selection cuts.

the background, by holding it at the level at $m_{\gamma\gamma} = 80$ GeV. Thus, our significance estimate would be somewhat conservative.

To obtain the signal diphoton distribution in the fiducial region we employ the selection cuts mentioned in Table 2. As for benchmark I, the kinematic cuts substantially reduce the number of events in the signal distribution, shown in Fig.10. Given the characteristic mass-splittings of this benchmark, we see that a large portion of the spectrum (consisting of 28 ALPs) in the diphoton distribution could potentially be resolved at the detector. Now, a bin-wise significance estimation, under the conservative assumption of the background events beyond $m_{\gamma\gamma} \approx 80$ GeV, leads to a distribution as shown in Fig.11 with a cumulative significance $S_{c,138} = 2.12\sigma$ over the signal region.

4.2.2 Benchmark Point II(b)

As the only modification we have in this case is the increase in the number of ALPs to $N = 40$, we follow the same strategy for the analysis as before. The signal's diphoton invariant mass distribution post acceptance cuts is shown in Fig.12. In contrast with the

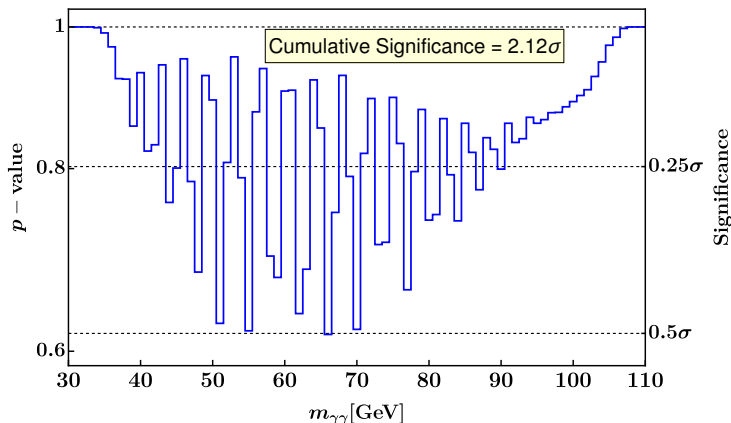


Figure 11: Bin-wise significance for benchmark II(a) at the LHC for $\mathcal{L} = 138 \text{ fb}^{-1}$.

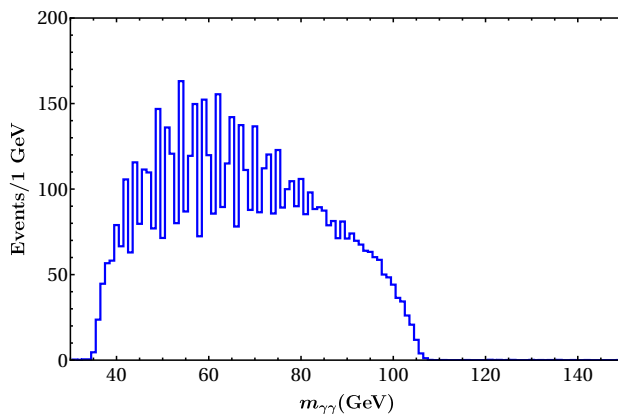


Figure 12: BP-II(b): Diphoton invariant mass distribution after applying acceptance cuts alone.

outcome for benchmark II(a), the sizes of the individual peaks have decreased, with the cross-sections scaling as $\sim |C_{nN}|^2/N$, and their smearing is now relatively more pronounced as a result of the smaller mass-splittings, both effected by the increase in the number of ALPs. The corresponding distribution in the fiducial region is presented in Fig.13, exhibiting, expectedly, the same signal shape as in Fig.12, although with a reduced number of events. The bin-wise significance estimate is shown in Fig.14 with the corresponding cumulative significance being $S_{c,138} = 1.97\sigma$.

Clearly, the two cases lead to slightly different projections for the 300 fb^{-1} luminosity reach, viz. $S_{c,300}^{(a)} \approx 3.12\sigma$ and $S_{c,300}^{(b)} \approx 2.9\sigma$. Thus, it may not be an overestimate to say that, upon a proper treatment, if the background distribution is found to saturate or slowly fall beyond $m_{\gamma\gamma} \sim 80 \text{ GeV}$, then benchmark II could also be potentially probed by the end of LHC's Run 3 phase.

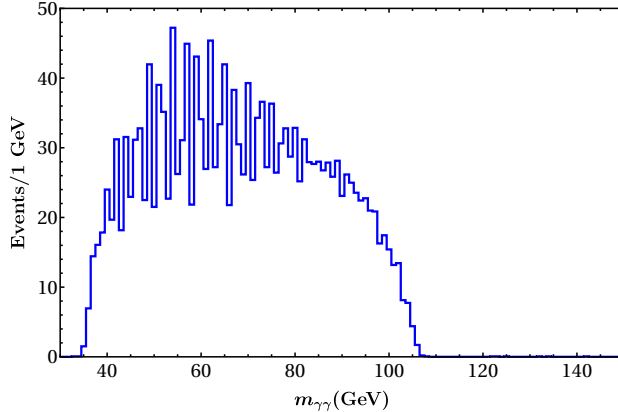


Figure 13: BP-II(b): Diphoton invariant mass distribution after applying selection cuts.

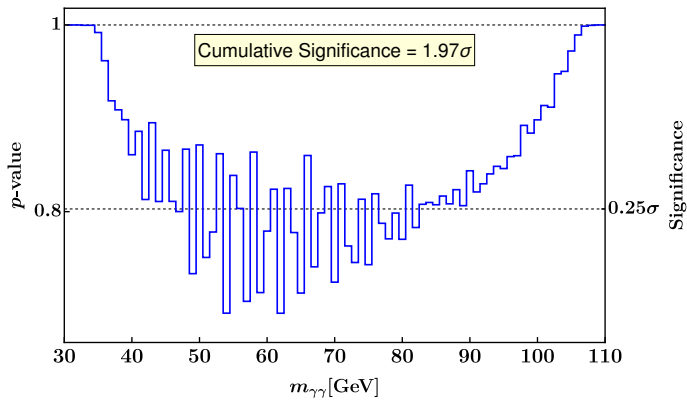


Figure 14: Bin-wise significance for benchmark II(b) at the LHC for $\mathcal{L} = 138 \text{ fb}^{-1}$.

4.3 Heavy ALPs

For ALPs that are significantly heavier than considered hitherto, the decay photons would be expected to carry sufficient energy (and p_T) for the event to be triggered even without any additional jet. An example is afforded by the aforementioned **Benchmark III**, wherein the ALP masses span the range $\sim 150 - 450 \text{ GeV}$. However, although extra jets are not needed for triggering, events with such jets do contribute significantly to the signal cross sections. Hence, we define the signal as a semi-inclusive one composed of a pair of energetic photons with upto two additional jets¹⁶. The corresponding K -factors, for this mass range, are taken from refs.[69, 90].

The background, thus, would receive contributions from essentially the same channels as assumed in the low mass case. The signal profile being different, we, though, would need to adequately tune the assessment, and, in this, we are guided by the ATLAS diphoton analysis [72] germane to this mass range. Post showering and hadronization, using `Pythia8`, we take for the identification and isolation of photons in the `Delphes` detector simulation a cone size of $\Delta R = 0.4$ around the photon candidate. The requirement on the parameter p_T^{ratio} ,

¹⁶The inclusion of three or more jets does not improve the signal to noise ratio.

Channel	Acceptance Cuts
	<u>Photon identification</u>
$pp \rightarrow a_n$	$\Delta R = 0.4, p_T > 0.4 \text{ GeV}, p_T^{\text{ratio}}(\gamma) < 0.12$
$a_n \rightarrow \gamma\gamma$	<u>Jet identification</u>
	$\Delta R = 0.4 \text{ (anti-}k_T), p_T^j > 20 \text{ GeV}, \eta_j < 2.5$
	<u>Isolation</u>
	$\Delta R(\gamma, \gamma) > 0.4, \Delta R(\gamma, j) > 0.4, \Delta R(j, j) > 0.7$
	$N_\gamma \geq 2$

Table 3: Acceptance cuts for the final state objects in benchmark III [72].

as defined earlier, is now reset to $p_T^{\text{ratio}} < 0.12$. The complete photon and jet identification criteria, as adapted from the ATLAS analysis ref.[72], are displayed in Table 3. The p_T distributions of the photons and the jets for the generated signal¹⁷ events are shown in Fig.15, adopting a bin size of 16 GeV as in the ATLAS search[72].

Fig.15 (right) shows the corresponding diphoton invariant mass distribution. Taking cue from ref.[72], we then apply the selection cuts mentioned in Table 4 in order to define the fiducial volume in the phase space.

Channel	Event Selection Criteria
	$N_\gamma = 2, N_j \leq 2$
$pp \rightarrow a_n$	$ \eta_\gamma < 2.37 \text{ (excluding barrel-to-endcap region } 1.37 < \eta_\gamma < 1.52),$
$a_n \rightarrow \gamma\gamma$	$E_T(\gamma_1) > 0.3 m_{\gamma\gamma}, E_T(\gamma_2) > 0.25 m_{\gamma\gamma}$
	$p_T^j > 20 \text{ GeV}, \eta_j < 2.5$

Table 4: Event selection cuts applied to form the fiducial signal regions for benchmark III [72].

The resulting diphoton invariant mass distribution is shown in Fig.16, whereas Fig.17 shows the corresponding bin-wise significance (with the background profile adopted from ref.[72]) over the diphoton signal region with a cumulative significance $S_{c,138} \approx 1.58\sigma$. For this case, the projected enhancement for a 300 fb^{-1} luminosity reach is $S_{c,300} \approx 2.33\sigma$. Thus, in contrast to benchmarks I and II, the high mass scenario will not be readily accessible in the LHC’s Run 3. It is perhaps worth speculating, though, that benchmark III, with heavy ALPs, could potentially reach the discovery threshold during the forthcoming high luminosity phase of the LHC with a projected luminosity enhancement by a factor of nearly 20 times the current value.

¹⁷In contrast with benchmarks I and II, events without jets in the final state also contribute significantly in this case and, therefore, $N_c(2j) < N_c(1j) < N_{Tot}$.

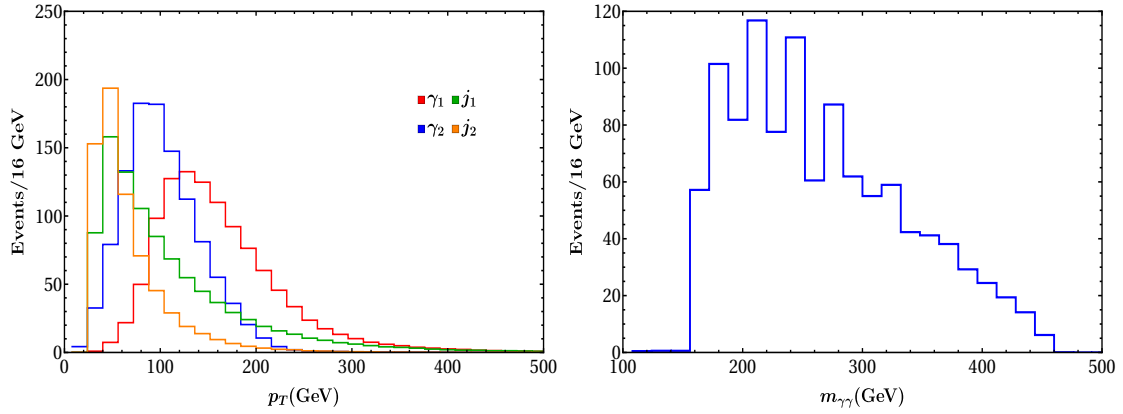


Figure 15: BP-III: event distributions, after applying acceptance cuts alone, *vide*. Table 3. **(left)** p_T distributions for the leading photon (γ_1), sub-leading photon (γ_2), leading jet (j_1) and the sub-leading jet (j_2) and **(right)** the two-photon invariant mass.

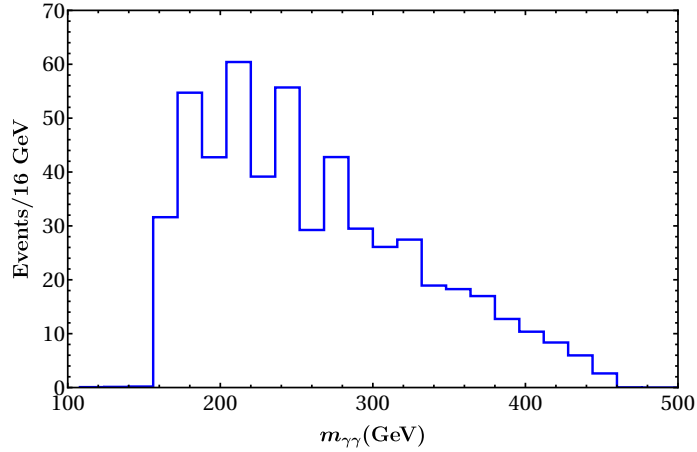


Figure 16: BP-III—Diphoton invariant mass distribution after applying selection cuts.

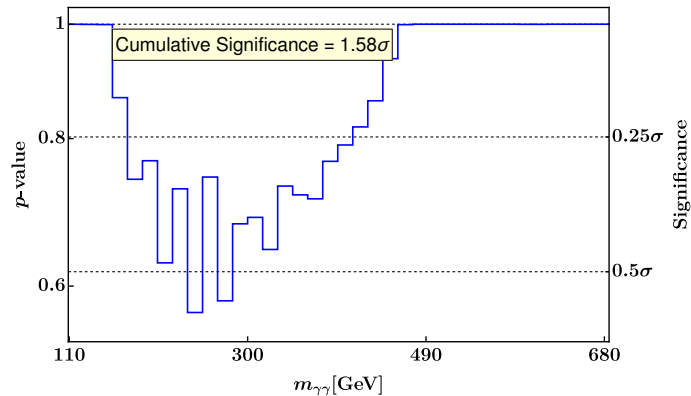


Figure 17: Bin-wise significance for benchmark III at the LHC for $\mathcal{L} = 138 \text{ fb}^{-1}$.

5 Vector-like quarks and heavy scalars

Beyond the low energy spectrum of the pseudoscalars, the model, as described in section 2, also contains a heavy quark with the $SU(3)_c \times SU(2)_L \times U(1)_Y$ charge assignment $(3, 1, 2/3)$ as well as $N + 1$ heavy radial scalar singlets (the partners of the pseudoscalars). Although not germane to the main objectives of our analysis, it is worth outlining here the dynamics of both the VLQ and the heavy scalars so as to establish the consistency of the model, especially in view of the fact that the assumed mass scales (characterised by the SSB scale f) of these heavy particles are, in principle, accessible at the LHC.

Considering that $m^2 \ll f^2$ in all the benchmarks, the off-diagonal quadratic terms for the radial scalars in the Lagrangian (eq.(2.4)) are hierarchically smaller than the diagonal mass terms governed by the coupling λ , which is presumed to assume $\mathcal{O}(1)$ values. Consequently, all the radial scalars are nearly degenerate with masses $\sim \sqrt{3\lambda}f$. To simplify matters, we assume the other new quartic coupling, *viz.* $\lambda_{\Phi H}$, is also small, thereby automatically relaxing constraints from the stability of the SM Higgs potential, triviality, etc. Similar to the pseudoscalars, these heavy scalars have effective interactions with the gluons, photons and the EW vector bosons with the respective couplings given by $g_{\pi V V}/\xi$, where $g_{\pi V V}$ represent the pseudoscalar couplings as listed in eq.(2.16).

As stated in the discussion following eq.(2.8), we assume, for the sake of simplicity, that the singlet VLQ mixes predominantly with the SM top quark, thereby automatically suppressing FCNCs involving the first two generations of quarks. Post-EWSB, the two quarks mix and the corresponding transformations can be expressed (in the limit of neglecting the very small mixings with the first two generations) as

$$\left(\Psi_L \quad u_L^{(3)}\right)^T = U \begin{pmatrix} T_L & t_L \end{pmatrix}^T, \quad \text{and} \quad \left(\Psi_R \quad u_R^{(3)}\right)^T = V \begin{pmatrix} T_R & t_R \end{pmatrix}^T, \quad (5.1)$$

where T, t represent the mass eigenstates and U, V are the (special unitary) mixing matrices. Since Ψ_R and $u_R^{(3)}$ have identical quantum numbers, there is no gauge-mediated FCNC involving T_R and t_R and the weak gauge couplings of the VLQ-like state T can be expressed as

$$\begin{aligned} \mathcal{L}_{T-V} = & \left(\frac{g}{\sqrt{2}}U_{tT}\right) W_\mu \bar{b}_L \gamma^\mu T_L + \left(\frac{g}{2c_w}U_{tt}^*U_{tT}\right) Z_\mu \bar{t}_L \gamma^\mu T_L \\ & + \frac{g}{c_w} Z_\mu \bar{T} \gamma^\mu \left[-\frac{2}{3}s_w^2 + \frac{g}{2c_w}U_{Tt}^*U_{tT}P_L\right] T + \text{h.c.} \end{aligned} \quad (5.2)$$

where $P_{L,R}$ are the usual chiral projection operators. On the other hand, the FCNCs involving the scalars, as derived from eq.(2.10), are given by

$$\begin{aligned} \mathcal{L}_{T-\phi} = & -\frac{1}{\sqrt{2}}\bar{t}_L [(\lambda_\Psi U_{tT}^* V_{TT} + y'_\Psi U_{tT}^* V_{tT}) \phi_N + (\lambda_h U_{tt}^* V_{tT} + y_\Psi U_{tt}^* V_{TT}) h] T_R \\ & -\frac{1}{\sqrt{2}}\bar{T}_L [(\lambda_\Psi U_{TT}^* V_{Tt} + y'_\Psi U_{TT}^* V_{tt}) \phi_N + (\lambda_h U_{Tt}^* V_{tt} + y_\Psi U_{Tt}^* V_{Tt}) h] t_R + \text{h.c.} \end{aligned} \quad (5.3)$$

To obtain the pseudoscalar FCNCs, it is perhaps the most convenient to make use of the shift symmetry and rescale the field $\Psi_L \rightarrow e^{i\xi\pi_N/f}\Psi_L$ in eq.(2.10). This, in turn, results in

a pseudovector FCNC term in the full Lagrangian through the kinetic term of the field Ψ_L , namely,

$$\mathcal{L}_{T-\pi} = \frac{\partial_\mu \pi_N}{f} \bar{T}_L \gamma^\mu (U_{TT}^* U_{Tt}) t_L + \text{h.c.}, \quad (5.4)$$

with π_N being expressed in terms of the mass eigenstates a_n through $\pi_N = \sum C_{Nk}^{-1} a_k$ with the matrix C as defined in eq.(2.6). For $f \gtrsim 1000$ GeV and $m_T \sim \lambda_\Psi f / \sqrt{2} > (m_{W,Z,h,\phi} + m_t)$, the primary decay channels for the VLQ are clearly $T \rightarrow bW$, $T \rightarrow tZ$, $T \rightarrow th$, $T \rightarrow t\phi_N$ (if kinematically allowed) and $T \rightarrow ta_n$ (see appendix B for the decay width expressions [91]). Note that the decays to the new scalars and pseudoscalars appear in addition to the conventional VLQ decay modes to the SM particles and, therefore, it is worth comparing the branching fractions pertaining to the different channels. As this needs specifying a few further parameters, we begin by doing so for each of the benchmark points:

BP-I and II: We assume $\lambda_\Psi = 2.2$, $y_\Psi = \epsilon y'_\Psi$, $\lambda = 1.8$ and $y'_\Psi \lesssim 0.1$ with $\epsilon = 0.1$. This choice of λ_Ψ is motivated by the experimental lower bound on the VLQ mass ($m_T \gtrsim 1500$ GeV) to be discussed below. However, as can be expected from such a large value of the coupling, the evolution is fast and an examination of the three-loop renormalization group equations [92] leads to the conclusion that the theory becomes a very strongly coupled one at a scale $\mu \sim 10$ TeV, signalling that new physics must take over well before this scale. Given that the clockwork model is *not* a UV-complete one, this, *per se*, may still be overlooked. However, we return to this point in the next section.

BP-III: The considerably larger value of the SSB scale f allows us the luxury of choosing a relatively smaller value for the Yukawa coupling λ_Ψ , and we consider, instead, $\lambda_\Psi = 1.5$, $\lambda = 0.7$ and $y_\Psi = \epsilon y'_\Psi$, $y'_\Psi \lesssim 0.1$ with $\epsilon = 0.1$. For such a choice, the running of λ_Ψ is significantly slower and the strong coupling phase of the theory lies near 10^8 GeV.

While in eqs.(5.2 & 5.3), we have not listed any alterations in the SM couplings of the top-quark, it is obvious that certain changes would be wrought. However, these changes are only higher-order in the T - u_3 mixing U_{tT} , and with the latter not being large, are well below the current sensitivity limits (the strongest being that for the SM CKM element V_{tb} [19]), whether from flavour physics or from top-decay.

The constraints on the VLQ sector would, thus, come from direct observations at colliders. At the large hadron collider, the overwhelmingly leading production mechanism is the QCD-driven one¹⁸. Once pair-produced, the T s would decay promptly. Table 5 lists the leading VLQ branching ratios for the three benchmark points¹⁹. It can be readily ascertained that the branching fractions have a very small dependence on the free parameter y'_Ψ .

As the table shows, the branching fractions relevant to the standard search algorithms are not overly affected. Consequently, the derived limits are only slightly relaxed at best. On the other hand, it might be interesting to consider exotic channels such as $T \rightarrow t + a_n \rightarrow t + \gamma\gamma$. Hitherto (largely) unexplored, these might be of interest at future runs of the LHC.

¹⁸With U_{tT} not being large, single production is suppressed and the consequent bounds [93] are relaxed.

¹⁹For the chosen set of couplings, a decay of T to radial scalars is kinematically forbidden. For any phenomenologically viable set of couplings, the branching fractions remain much smaller than those listed in the table.

Channel	Branching Ratios		
	SM	BP-I & II	BP-III
$T \rightarrow bW$	0.5	0.44	0.47
$T \rightarrow tZ$	0.25	0.21	0.23
$T \rightarrow th$	0.25	0.23	0.25
$T \rightarrow ta_{(\text{all})}$	—	0.12	0.05
m_T lower limit	1540 GeV [94, 95]	1500 GeV	≈ 1540 GeV

Table 5: VLQ branching fractions for BP-I,II and III (The SM column refers to the assumed branching fractions for VLQ searches [93, 94]). The bottom row displays the resulting lower bounds on m_T , as derived from the limits on the VLQ pair-production cross-section presented in ref.[94]

6 Summary and Conclusion

We have examined the minimal QCD axion model within the *clockwork* paradigm and investigated the prospects of observing the massive ALPs that the model engenders at current and future hadron colliders. To this end, we employ a KSVZ-like setup with a heavy $SU(2)_L$ singlet quark (as a top-partner) which couples to the CW sector at the site $j = N$ through an analogue of the PQ symmetry and naturally addresses the strong CP problem in the traditional manner. Thus, the lightest pNGB in the CW sector identifies as the QCD axion while the accompanying heavier pNGBs in the spectrum behave as ALPs with a characteristic mass scale $\sim mq$. Through the chiral anomaly, these axions then couple to the gluons, the photon and the Z boson, albeit with hierarchically different decay constants for the QCD axion and the ALPs, namely $f_0 \sim q^{-N}f$ and $f_{n>0} \sim f$, thanks to the CW mechanism. Being naturally consistent with the current experimental and observational constraints, the large suppression in the effective couplings of the light axion renders it practically invisible at high energy colliders. Therefore, for a reasonable parameter configuration such as $q > 1$, $N \sim \mathcal{O}(10)$, $m \gtrsim 10$ GeV and $f \sim 1$ TeV, what seems more plausible instead is the production and detection of the ALPs, especially at hadron colliders such as the currently operating LHC and its future derivatives. To perform a quantitative analysis, we classify three benchmark scenarios according to the ALP masses in the range 10 – 30 GeV (BP-I), 35 – 105 GeV (BP-II) and 150 – 450 GeV (BP-III). Such varied mass scales for the ALPs is enabled by the fact that the CW mechanism is based on the premise of localization in the theory space and, thus, is practically independent of the mass scales assumed in the theory. We performed an analysis of the expected signal profiles pertaining to the three benchmark points for the production of ALPs (with upto two additional jets) via gluon fusion and their subsequent decay to two photons at the LHC for an integrated luminosity of 138 fb^{-1} . As anchor points for the analysis and for estimates of the pertinent background distributions, we referred to the ATLAS searches for diphoton resonances in the relevant invariant mass regions [71, 72]. What stands out as particularly interesting is the case of the light ALPs where the number of particles N that is consistent

with the QCD axion being a dark matter candidate also induces very small mass-splittings among the ALPs. The resulting diphoton invariant mass distribution for the signal events turns out to be such that the individual resonances are smeared by the detector’s resolution (implemented in the form of a fast simulation of the ATLAS detector) and, thereby, overlap with each other to a certain extent. Therefore, such scenarios suggest that the existence of a CW spectrum of light ALPs might, in principle, also manifest in the observation of a single broad resonance instead of the typical signatures of distinct, well-separated, resonances. Treating the spectrum as a whole also offers the possibility of a better, more inclusive, estimation of the signal’s statistical significance over the background. For instance, the simplistic *cumulative* estimation defined in this work gives a sizable significance value of $S_c \sim 3.4\sigma$ in BP-I, even though the significance estimates of the individual bins in the signal distribution are comparatively small. Moreover, when scaled by the projected luminosity reach of the ongoing Run 3 phase of the LHC, *viz.* $\sim 300 \text{ fb}^{-1}$, the cumulative significance gets enhanced to $S_c \sim 5\sigma$. Of course, a dedicated search for such signals would call for a more detailed statistical analysis that is tailored to the fact that the individual resonances of the CW spectrum are characteristically correlated. As for the heavy ALPs, e.g. those encountered in BP-III, one may not be very hopeful within the LHC era, with the cumulative significance falling below 3σ even at the 300 fb^{-1} level. What is exciting, though, is the prospect of probing a wide window of the CW ALPs at the HL-LHC with a planned luminosity reach of $\sim 3000 \text{ fb}^{-1}$, where larger portions of the diphoton invariant mass profile could start to become apparent — the structure of the axion *iceberg* revealing itself — and even scenarios like BP-III could possibly surpass the discovery threshold.

A key issue in our analysis has been the opposing pull on the SSB scale f from the need to increase the effective ALP–gluon–gluon coupling (scaling as f^{-1}) on the one hand and the lower bound on the VLQ mass (scaling as f) on the other. While modifying the number of sites N , or the exponent parameter q does make a difference, the effect is a muted one (especially given that renormalizability of the low energy theory requires that $q \leq 3$). However, given that the light ALP solutions presented here (benchmark points I & II) indicate that further new physics must exist by $\sim 10 \text{ TeV}$ scale, such a restriction might seem unwarranted and $q > 3$ may be considered. However, since the ALP couplings to the gluons and photon have a dependence on q which appears only through the elements of the CW transformation matrix, namely $C_{(n>0)N}$, the corresponding gain is marginal. It can be similarly argued that a change in the position of the VLQ coupling over the CW lattice (*i.e.*, to assume $j < N$) also does not lead to a substantial gain.

Naively, a second possibility would be to postulate additional VLQs such that the effective $a_n gg$ coupling may be raised by way of all the VLQs contributing in the loop diagram. However, the corresponding change in the axion potential would putatively lead to the formation of stable domain walls in the early Universe and is phenomenologically disfavoured. While one might attempt to mitigate the issue by invoking some of the solutions proposed in the literature, e.g. by assuming a soft breaking of the discrete symmetry or an inflation-induced statistical bias in the axion potential, the model would, nevertheless, be severely constrained due to the inherent drawbacks of such solutions [96]. Consider, instead, the introduction of a one (or more) vector-like lepton (VLL). This, then, does not contribute

to the $a_n gg$ couplings (thereby evading the domain wall constraints), but does contribute to the $a_n \gamma \gamma$ couplings, which now get enhanced by a factor of

$$1 + \frac{1}{3Y_\Psi^2} \sum N_L Q_L^2$$

where N_L is the number of VLLs of charge Q_L . Even the simplest choice of a single VLL of charge $Q = -1$ enhances the coupling by a factor of 1.75, thereby allowing on a similar enhancement in f without changing the rates. This, in turn, allows for a smaller Yukawa λ_Ψ , and postponement of the strong coupling phase until a cutoff scale $\mu \gtrsim 10^7$ GeV. As for the VLL phenomenology, the LHC limits are understandably much weaker. For it to decay, it must have at least a small Yukawa coupling with a SM lepton, and postulating this to be the τ would not only escape low-energy constraints, but also allow for intriguing signals at the LHC.

An entirely different mechanism of raising f without suppressing the signal is afforded by the choice of the $U(1)_N$ charge ξ for the Ψ_L and Φ_N . Increasing ξ and f proportionately keeps f_{eff} (and, therefore, the $a_n gg$ coupling) unchanged.

Whatever such mechanisms may be, it is quite apparent that the clockwork-axion-ALP scenario would be manifested at the LHC in terms of interesting signals, perhaps the most interesting being the case of the strong coupling phase itself.

A The axial anomaly

In the KSVZ model described in this work, the left and the right-handed projections of the heavy fermion Ψ are chirally charged under the global symmetry $U(1)_N$. As is usually the case in KSVZ models, the chiral (or axial) $U(1)_N$ (analogous to $U(1)_{PQ}$ in the original setup) symmetry is anomalous which, in turn, results in the couplings of the pseudoscalar π_N to gluons and the hypercharge boson given in eq.(2.11). This is most succinctly realized in the path integral formulation of the KSVZ theory, with the partition function given by

$$Z[0]_A = \int \mathcal{D}\bar{\Psi} \mathcal{D}\Psi \exp \left[i \int d^4x \mathcal{L}_\Psi \right]. \quad (\text{A.1})$$

Here, the subscript A denotes a fixed background with respect to the gauge fields and $\mathcal{L}_\Psi[\Psi, \bar{\Psi}, D_\mu \Psi, D_\mu \bar{\Psi}]$ marks the full Lagrangian for Ψ including the kinetic terms as well. Post SSB (at the scale f), the Yukawa term for Ψ given in eq.(2.10) (ignoring the mixing terms with the SM fermions for brevity) can be rewritten in the convenient form

$$-\frac{\lambda_\Psi}{\sqrt{2}} (\phi + f) e^{i\xi \pi_N \gamma_5 / f} \bar{\Psi} \Psi. \quad (\text{A.2})$$

The anomalous nature of $U(1)_N$ is apparent when we see that while the tree level action is invariant under the chiral transformation

$$\Psi' = U\Psi = e^{-i\xi\beta\gamma_5/(2f)}\Psi, \quad \pi_N \rightarrow \pi_N + \beta, \quad (\text{A.3})$$

where β is a constant transformation parameter, the measure of the path integral is not. The measure would transform as,

$$\mathcal{D}\bar{\Psi}\mathcal{D}\Psi \rightarrow |\mathcal{J}|^{-2}\mathcal{D}\bar{\Psi}\mathcal{D}\Psi, \quad (\text{A.4})$$

where \mathcal{J} is the Jacobian corresponding to the chiral transformation. The Jacobian, after appropriate regularisation, is given by [97, 98]

$$\mathcal{J} = \frac{i}{64\pi^2} \exp \left[\int d^4x \frac{\xi\beta}{f} \text{Tr}\{F^{\mu\nu}\tilde{F}_{\mu\nu}\} \right]. \quad (\text{A.5})$$

where $F^{\mu\nu}\tilde{F}_{\mu\nu} \equiv F^{A\mu\nu}\tilde{F}_{\mu\nu}^B T^A T^B$ which stands for the gauge fields for all the local symmetries under which Ψ is charged with T^A being the respective generators. For brevity, we define T^A such that they include the corresponding gauge couplings. Tr denotes trace over the gauge representation of the field Ψ . Therefore, the anomaly term which appears in the full Lagrangian is given by

$$\mathcal{A}(x) = -\frac{\xi\beta}{32\pi^2 f} \text{Tr}\{F^{\mu\nu}\tilde{F}_{\mu\nu}\}. \quad (\text{A.6})$$

Similarly, if we use the freedom to redefine the field Ψ so as to absorb the pseudoscalar field through the chiral transformation

$$\Psi \rightarrow e^{-i\xi\pi_N\gamma_5/(2f)}\Psi, \quad (\text{A.7})$$

we obtain the corresponding anomaly term in the Lagrangian given by

$$\mathcal{A}(x) = -\frac{\xi\pi_N}{32\pi^2 f} \text{Tr}\{F^{\mu\nu}\tilde{F}_{\mu\nu}\}. \quad (\text{A.8})$$

A straightforward evaluation of the trace in the preceding expression leads to the terms in eq.(2.11).

B VLQ decay widths

In the following we list the decay width expressions for the heavy fermion Ψ with the labels q and V denoting the SM quarks (b, t) and the EW gauge bosons (W, Z) respectively.

$$\begin{aligned} \Gamma(T \rightarrow qV) &= |g_L^V|^2 \frac{\sqrt{m_q^4 - 2m_q^2(m_T^2 + m_V^2) + (m_T^2 - m_V^2)^2}}{32\pi m_T^3 m_V^2} \\ &\quad \left[(m_T^2 - m_q^2)^2 + m_V^2(m_T^2 + m_q^2) - 2m_V^4 \right] \\ &\approx \frac{|g_L^V|^2 m_T^3}{32\pi m_V^2} \quad (\text{for } m_T \gg m_{q,V}) \quad . \end{aligned} \quad (\text{B.1})$$

Here, the couplings g_L^V are given by

$$g_L^W = \frac{g}{\sqrt{2}}U_{tT}, \quad g_L^Z = \frac{1}{2}\frac{g}{c_w}U_{tt}^*U_{tT}, \quad (\text{B.2})$$

whereas the corresponding (off-diagonal) right-handed couplings vanish identically thanks to an analogue of the GIM mechanism.

For decays to scalars we ignore the small mixing between the SM Higgs and the heavy scalars ϕ_n . The corresponding expressions are

$$\begin{aligned}\Gamma(T \rightarrow t h) &= \frac{\sqrt{m_h^4 - 2m_h^2(m_T^2 + m_t^2) + (m_T^2 - m_t^2)^2}}{64\pi m_T^3} \\ &\times \left\{ (|y_{Tt}^h|^2 + |y_{tT}^h|^2) [m_T^2 + m_t^2 - m_h^2] + 2(y_{Tt}^{h*} y_{tT}^h + y_{tT}^h y_{Tt}^{h*}) m_T m_t \right\} \quad (\text{B.3}) \\ &\approx \frac{(|y_{Tt}^h|^2 + |y_{tT}^h|^2)}{64\pi} m_T \quad (\text{for } m_T \gg m_{t,h}),\end{aligned}$$

$$\begin{aligned}\Gamma(T \rightarrow t \phi_N) &= \frac{\sqrt{m_{\phi_N}^4 - 2m_{\phi_N}^2(m_T^2 + m_t^2) + (m_T^2 - m_t^2)^2}}{64\pi m_T^3} \\ &\times \left\{ (|y_{Tt}^\Phi|^2 + |y_{tT}^\Phi|^2) [m_T^2 + m_t^2 - m_{\phi_N}^2] + 2(y_{Tt}^{\Phi*} y_{tT}^\Phi + y_{tT}^\Phi y_{Tt}^{\Phi*}) m_T m_t \right\} \quad (\text{B.4}) \\ &\approx \frac{(|y_{Tt}^\Phi|^2 + |y_{tT}^\Phi|^2)}{64\pi} m_T \left(1 - 2\frac{m_{\phi_N}^2}{m_T^2} + \frac{m_{\phi_N}^4}{m_T^4} \right) \quad (\text{for } m_{T,\phi_N} \gg m_t)\end{aligned}$$

and

$$\begin{aligned}\Gamma(T \rightarrow t a_n) &= \frac{\xi^2 C_{nN}^2 \sqrt{m_n^4 - 2m_n^2(m_T^2 + m_t^2) + (m_T^2 - m_t^2)^2}}{32\pi f^2 m_T^3} \\ &\quad (|U_{TT}|^2 |U_{Tt}|^2) \left[(m_T^2 - m_t^2)^2 - (m_T^2 + m_t^2) m_n^2 \right] \quad (\text{B.5}) \\ &\approx \frac{\lambda_\Psi^2 \xi^2 C_{nN}^2 |U_{TT}|^2 |U_{Tt}|^2}{32\pi} m_T \quad (\text{for } m_T \gg m_{t,a_n}),\end{aligned}$$

where the effective Yukawa couplings are given by

$$\begin{aligned}y_{Tt}^h &\approx \lambda_h U_{Tt}^* V_{tt}, & y_{tT}^h &= \lambda_h U_{tt}^* V_{tT} + y_\Psi U_{tt}^* V_{TT}, \\ y_{tT}^\Phi &\approx \lambda_\Psi U_{tT}^* V_{TT}, & y_{Tt}^\Phi &= \lambda_\Psi U_{TT}^* V_{Tt} + y'_\Psi U_{TT}^* V_{tt}.\end{aligned} \quad (\text{B.6})$$

Acknowledgments

The authors thank Satyaki Bhattacharya for helpful discussions. S.M. acknowledges research Grant No. CRG/2018/004889 of the SERB, India. T.S. acknowledges the support from the Dr. D.S. Kothari Postdoctoral fellowship scheme no. F.4-2/2006 (BSR)/PH/20-21/0163.

References

- [1] R.D. Peccei and H.R. Quinn, CP conservation in the presence of pseudoparticles, *Phys. Rev. Lett.* **38** (1977) 1440.
- [2] S. Weinberg, A new light boson?, *Phys. Rev. Lett.* **40** (1978) 223.

- [3] F. Wilczek, *Problem of strong p and t invariance in the presence of instantons*, *Phys. Rev. Lett.* **40** (1978) 279.
- [4] H. Georgi and I.N. McArthur, *INSTANTONS AND THE u QUARK MASS*, 1981.
- [5] D.B. Kaplan and A.V. Manohar, *Current Mass Ratios of the Light Quarks*, *Phys. Rev. Lett.* **56** (1986) 2004.
- [6] K. Choi, C.W. Kim and W.K. Sze, *Mass Renormalization by Instantons and the Strong CP Problem*, *Phys. Rev. Lett.* **61** (1988) 794.
- [7] T. Banks, Y. Nir and N. Seiberg, *Missing (up) mass, accidental anomalous symmetries, and the strong CP problem*, in *2nd IFT Workshop on Yukawa Couplings and the Origins of Mass*, pp. 26–41, 2, 1994 [[hep-ph/9403203](#)].
- [8] M. Dine, P. Draper and G. Festuccia, *Instanton Effects in Three Flavor QCD*, *Phys. Rev. D* **92** (2015) 054004 [[1410.8505](#)].
- [9] A.E. Nelson, *Naturally Weak CP Violation*, *Phys. Lett. B* **136** (1984) 387.
- [10] S.M. Barr, *Solving the Strong CP Problem Without the Peccei-Quinn Symmetry*, *Phys. Rev. Lett.* **53** (1984) 329.
- [11] C. Alexandrou, J. Finkenrath, L. Funcke, K. Jansen, B. Kostrzewa, F. Pittler et al., *Ruling Out the Massless Up-Quark Solution to the Strong CP Problem by Computing the Topological Mass Contribution with Lattice QCD*, *Phys. Rev. Lett.* **125** (2020) 232001 [[2002.07802](#)].
- [12] M. Dine and P. Draper, *Challenges for the Nelson-Barr Mechanism*, *JHEP* **08** (2015) 132 [[1506.05433](#)].
- [13] G. Lazarides and Q. Shafi, *Axion Models with No Domain Wall Problem*, *Phys. Lett. B* **115** (1982) 21.
- [14] C. Chatterjee, T. Higaki and M. Nitta, *Note on a solution to domain wall problem with the Lazarides-Shafi mechanism in axion dark matter models*, *Phys. Rev. D* **101** (2020) 075026 [[1903.11753](#)].
- [15] M. Ibe, S. Kobayashi, M. Suzuki and T.T. Yanagida, *Dynamical solution to the axion domain wall problem*, *Phys. Rev. D* **101** (2020) 035029 [[1909.01604](#)].
- [16] Y. Zhang, *Imperfect Axion Precludes the Domain Wall Problem*, *Phys. Rev. Lett.* **132** (2024) 081003 [[2305.15495](#)].
- [17] L.D. Duffy and K. van Bibber, *Axions as Dark Matter Particles*, *New J. Phys.* **11** (2009) 105008 [[0904.3346](#)].
- [18] F. Chadha-Day, J. Ellis and D.J.E. Marsh, *Axion dark matter: What is it and why now?*, *Sci. Adv.* **8** (2022) abj3618 [[2105.01406](#)].
- [19] PARTICLE DATA GROUP collaboration, *Review of particle physics*, *Phys. Rev. D* **110** (2024) 030001.
- [20] C. O’Hare, “cajohare/axionlimits: Axionlimits.” <https://cajohare.github.io/AxionLimits/>, July, 2020. 10.5281/zenodo.3932430.
- [21] M. Bauer, M. Heiles, M. Neubert and A. Thamm, *Axion-Like Particles at Future Colliders*, *Eur. Phys. J. C* **79** (2019) 74 [[1808.10323](#)].
- [22] D. d’Enterria, *Collider constraints on axion-like particles*, in *Workshop on Feebly Interacting Particles*, 2, 2021 [[2102.08971](#)].

- [23] A. Flórez, A. Gurrrola, W. Johns, P. Sheldon, E. Sheridan, K. Sinha et al., *Probing axionlike particles with $\gamma\gamma$ final states from vector boson fusion processes at the LHC*, *Phys. Rev. D* **103** (2021) 095001 [[2101.11119](#)].
- [24] V.A. Rubakov, *Grand unification and heavy axion*, *JETP Lett.* **65** (1997) 621 [[hep-ph/9703409](#)].
- [25] Z. Berezhiani, L. Gianfagna and M. Giannotti, *Strong CP problem and mirror world: The Weinberg-Wilczek axion revisited*, *Phys. Lett. B* **500** (2001) 286 [[hep-ph/0009290](#)].
- [26] H. Fukuda, K. Harigaya, M. Ibe and T.T. Yanagida, *Model of visible QCD axion*, *Phys. Rev. D* **92** (2015) 015021 [[1504.06084](#)].
- [27] A. Hook, S. Kumar, Z. Liu and R. Sundrum, *High Quality QCD Axion and the LHC*, *Phys. Rev. Lett.* **124** (2020) 221801 [[1911.12364](#)].
- [28] P. Agrawal and K. Howe, *Factoring the Strong CP Problem*, *JHEP* **12** (2018) 029 [[1710.04213](#)].
- [29] T. Gherghetta, V.V. Khoze, A. Pomarol and Y. Shirman, *The Axion Mass from 5D Small Instantons*, *JHEP* **03** (2020) 063 [[2001.05610](#)].
- [30] T. Flacke, B. Gripaios, J. March-Russell and D. Maybury, *Warped axions*, *JHEP* **01** (2007) 061 [[hep-ph/0611278](#)].
- [31] D.E. Kaplan and R. Rattazzi, *Large field excursions and approximate discrete symmetries from a clockwork axion*, *Phys. Rev. D* **93** (2016) 085007 [[1511.01827](#)].
- [32] K. Choi and S.H. Im, *Realizing the relaxation from multiple axions and its UV completion with high scale supersymmetry*, *JHEP* **01** (2016) 149 [[1511.00132](#)].
- [33] G.F. Giudice and M. McCullough, *A Clockwork Theory*, *JHEP* **02** (2017) 036 [[1610.07962](#)].
- [34] M. Farina, D. Pappadopulo, F. Rompineve and A. Tesi, *The photo-philic QCD axion*, *JHEP* **01** (2017) 095 [[1611.09855](#)].
- [35] T. Higaki, K.S. Jeong, N. Kitajima and F. Takahashi, *The QCD Axion from Aligned Axions and Diphoton Excess*, *Phys. Lett. B* **755** (2016) 13 [[1512.05295](#)].
- [36] J.E. Kim, *Weak Interaction Singlet and Strong CP Invariance*, *Phys. Rev. Lett.* **43** (1979) 103.
- [37] M.A. Shifman, A.I. Vainshtein and V.I. Zakharov, *Can Confinement Ensure Natural CP Invariance of Strong Interactions?*, *Nucl. Phys. B* **166** (1980) 493.
- [38] M. Kamionkowski and J. March-Russell, *Planck scale physics and the Peccei-Quinn mechanism*, *Phys. Lett. B* **282** (1992) 137 [[hep-th/9202003](#)].
- [39] L. Randall, *Composite axion models and Planck scale physics*, *Phys. Lett. B* **284** (1992) 77.
- [40] I. Ben-Dayan, *Generalized Clockwork Theory*, *Phys. Rev. D* **99** (2019) 096006 [[1706.05308](#)].
- [41] A. Banerjee, S. Ghosh and T.S. Ray, *Clockworked VEVs and Neutrino Mass*, *JHEP* **11** (2018) 075 [[1808.04010](#)].
- [42] G. Alonso-Álvarez, M.B. Gavela and P. Quilez, *Axion couplings to electroweak gauge bosons*, *Eur. Phys. J. C* **79** (2019) 223 [[1811.05466](#)].
- [43] G. Grilli di Cortona, E. Hardy, J. Pardo Vega and G. Villadoro, *The QCD axion, precisely*, *JHEP* **01** (2016) 034 [[1511.02867](#)].

- [44] PARTICLE DATA GROUP collaboration, *Review of Particle Physics*, *PTEP* **2022** (2022) 083C01.
- [45] I. Schulthess et al., *New Limit on Axionlike Dark Matter Using Cold Neutrons*, *Phys. Rev. Lett.* **129** (2022) 191801 [2204.01454].
- [46] C. Abel et al., *Search for Axionlike Dark Matter through Nuclear Spin Precession in Electric and Magnetic Fields*, *Phys. Rev. X* **7** (2017) 041034 [1708.06367].
- [47] T.S. Roussy et al., *Experimental Constraint on Axionlike Particles over Seven Orders of Magnitude in Mass*, *Phys. Rev. Lett.* **126** (2021) 171301 [2006.15787].
- [48] E. Madge, G. Perez and Z. Meir, *Prospects of nuclear-coupled-dark-matter detection via correlation spectroscopy of I_2^+ and Ca^+* , 2404.00616.
- [49] X. Zhang, A. Banerjee, M. Leyser, G. Perez, S. Schiller, D. Budker et al., *Search for Ultralight Dark Matter with Spectroscopy of Radio-Frequency Atomic Transitions*, *Phys. Rev. Lett.* **130** (2023) 251002 [2212.04413].
- [50] P.J. Fox, N. Weiner and H. Xiao, *Recurrent axion stars collapse with dark radiation emission and their cosmological constraints*, *Phys. Rev. D* **108** (2023) 095043 [2302.00685].
- [51] K. Blum, R.T. D’Agnolo, M. Lisanti and B.R. Safdi, *Constraining Axion Dark Matter with Big Bang Nucleosynthesis*, *Phys. Lett. B* **737** (2014) 30 [1401.6460].
- [52] V.M. Mehta, M. Demirtas, C. Long, D.J.E. Marsh, L. Mcallister and M.J. Stott, *Superradiance Exclusions in the Landscape of Type IIB String Theory*, 2011.08693.
- [53] M. Baryakhtar, M. Galanis, R. Lasenby and O. Simon, *Black hole superradiance of self-interacting scalar fields*, *Phys. Rev. D* **103** (2021) 095019 [2011.11646].
- [54] C. Ünal, F. Pacucci and A. Loeb, *Properties of ultralight bosons from heavy quasar spins via superradiance*, *JCAP* **05** (2021) 007 [2012.12790].
- [55] A. Hook and J. Huang, *Probing axions with neutron star inspirals and other stellar processes*, *JHEP* **06** (2018) 036 [1708.08464].
- [56] J. Zhang, Z. Lyu, J. Huang, M.C. Johnson, L. Sagunski, M. Sakellariadou et al., *First Constraints on Nuclear Coupling of Axionlike Particles from the Binary Neutron Star Gravitational Wave Event GW170817*, *Phys. Rev. Lett.* **127** (2021) 161101 [2105.13963].
- [57] L. Caloni, M. Gerbino, M. Lattanzi and L. Visinelli, *Novel cosmological bounds on thermally-produced axion-like particles*, *JCAP* **09** (2022) 021 [2205.01637].
- [58] G. Lucente, L. Mastrototaro, P. Carena, L. Di Luzio, M. Giannotti and A. Mirizzi, *Axion signatures from supernova explosions through the nucleon electric-dipole portal*, *Phys. Rev. D* **105** (2022) 123020 [2203.15812].
- [59] R. Balkin, J. Serra, K. Springmann, S. Stelzl and A. Weiler, *White dwarfs as a probe of exceptionally light QCD axions*, *Phys. Rev. D* **109** (2024) 095032 [2211.02661].
- [60] S.M. Barr, K. Choi and J.E. Kim, *Some aspects of axion cosmology in unified and superstring models*, *Nucl. Phys. B* **283** (1987) 591.
- [61] J.E. Kim, *Light Pseudoscalars, Particle Physics and Cosmology*, *Phys. Rept.* **150** (1987) 1.
- [62] S. Chang, C. Hagmann and P. Sikivie, *Studies of the motion and decay of axion walls bounded by strings*, *Phys. Rev. D* **59** (1999) 023505 [hep-ph/9807374].

- [63] P. Sikivie, *Of Axions, Domain Walls and the Early Universe*, *Phys. Rev. Lett.* **48** (1982) 1156.
- [64] Y.K. Semertzidis and S. Youn, *Axion dark matter: How to see it?*, *Sci. Adv.* **8** (2022) abm9928 [2104.14831].
- [65] A. Mariotti, D. Redigolo, F. Sala and K. Tobioka, *New LHC bound on low-mass diphoton resonances*, *Phys. Lett. B* **783** (2018) 13 [1710.01743].
- [66] R.D. Ball, M. Bonvini, S. Forte, S. Marzani and G. Ridolfi, *Higgs production in gluon fusion beyond NNLO*, *Nucl. Phys. B* **874** (2013) 746 [1303.3590].
- [67] M. Bonvini, R.D. Ball, S. Forte, S. Marzani and G. Ridolfi, *Updated Higgs cross section at approximate N^3LO* , *J. Phys. G* **41** (2014) 095002 [1404.3204].
- [68] M. Bonvini, S. Marzani, C. Muselli and L. Rottoli, *On the Higgs cross section at N^3LO+N^3LL and its uncertainty*, *JHEP* **08** (2016) 105 [1603.08000].
- [69] T. Ahmed, M. Bonvini, M.C. Kumar, P. Mathews, N. Rana, V. Ravindran et al., *Pseudo-scalar Higgs boson production at $N^3 LO_A + N^3 LL'$* , *Eur. Phys. J. C* **76** (2016) 663 [1606.00837].
- [70] A. Djouadi, *The Anatomy of electro-weak symmetry breaking. I: The Higgs boson in the standard model*, *Phys. Rept.* **457** (2008) 1 [hep-ph/0503172].
- [71] ATLAS collaboration, *Search for boosted diphoton resonances in the 10 to 70 GeV mass range using 138 fb^{-1} of 13 TeV pp collisions with the ATLAS detector*, *JHEP* **07** (2023) 155 [2211.04172].
- [72] ATLAS collaboration, *Search for resonances decaying into photon pairs in 139 fb^{-1} of pp collisions at $\sqrt{s}=13$ TeV with the ATLAS detector*, *Phys. Lett. B* **822** (2021) 136651 [2102.13405].
- [73] ATLAS collaboration, *Search for diphoton resonances in the 66 to 110 GeV mass range using 140 fb^{-1} of 13 TeV pp collisions collected with the ATLAS detector*, Tech. Rep. **ATLAS-CONF-2023-035**, CERN, Geneva (2023).
- [74] CMS collaboration, *Search for a standard model-like Higgs boson in the mass range between 70 and 110 GeV in the diphoton final state in proton-proton collisions at $\sqrt{s} = 13$ TeV*, Tech. Rep. **CMS-PAS-HIG-20-002**, CERN, Geneva (2023).
- [75] CMS collaboration, *Search for new physics in high-mass diphoton events from proton-proton collisions at $\sqrt{s} = 13$ TeV*, Tech. Rep. **CMS-PAS-EXO-22-024**, CERN, Geneva (2024).
- [76] G. Alonso-Álvarez, J.M. Cline and T. Xiao, *The flavor of QCD axion dark matter*, *JHEP* **07** (2023) 187 [2305.00018].
- [77] NNPDF collaboration, *Parton distributions for the LHC Run II*, *JHEP* **04** (2015) 040 [1410.8849].
- [78] A. Alloul, N.D. Christensen, C. Degrande, C. Duhr and B. Fuks, *FeynRules 2.0 - A complete toolbox for tree-level phenomenology*, *Comput. Phys. Commun.* **185** (2014) 2250 [1310.1921].
- [79] J. Alwall, R. Frederix, S. Frixione, V. Hirschi, F. Maltoni, O. Mattelaer et al., *The automated computation of tree-level and next-to-leading order differential cross sections, and their matching to parton shower simulations*, *JHEP* **07** (2014) 079 [1405.0301].
- [80] T. Sjöstrand, S. Ask, J.R. Christiansen, R. Corke, N. Desai, P. Ilten et al., *An introduction to PYTHIA 8.2*, *Comput. Phys. Commun.* **191** (2015) 159 [1410.3012].

- [81] C. Bierlich et al., *A comprehensive guide to the physics and usage of PYTHIA 8.3*, *SciPost Phys. Codeb.* **2022** (2022) 8 [[2203.11601](#)].
- [82] DELPHES 3 collaboration, *DELPHES 3, A modular framework for fast simulation of a generic collider experiment*, *JHEP* **02** (2014) 057 [[1307.6346](#)].
- [83] P. Artoisenet, R. Frederix, O. Mattelaer and R. Rietkerk, *Automatic spin-entangled decays of heavy resonances in Monte Carlo simulations*, *JHEP* **03** (2013) 015 [[1212.3460](#)].
- [84] M. Cacciari, G.P. Salam and G. Soyez, *FastJet User Manual*, *Eur. Phys. J. C* **72** (2012) 1896 [[1111.6097](#)].
- [85] M. Cacciari, G.P. Salam and G. Soyez, *The anti- k_t jet clustering algorithm*, *JHEP* **04** (2008) 063 [[0802.1189](#)].
- [86] Y. Gershtein, S. Knapen and D. Redigolo, *Probing naturally light singlets with a displaced vertex trigger*, *Phys. Lett. B* **823** (2021) 136758 [[2012.07864](#)].
- [87] E. Conte, B. Fuks and G. Serret, *MadAnalysis 5, A User-Friendly Framework for Collider Phenomenology*, *Comput. Phys. Commun.* **184** (2013) 222 [[1206.1599](#)].
- [88] M. Aharrouche, J. Colas, L. Di Ciaccio, M. El Kacimi, O. Gaumer, M. Gouanère et al., *Energy linearity and resolution of the atlas electromagnetic barrel calorimeter in an electron test-beam*, *Nuclear Instruments and Methods in Physics Research Section A: Accelerators, Spectrometers, Detectors and Associated Equipment* **568** (2006) 601.
- [89] ATLAS collaboration, *Search for diphoton resonances in the 66 to 110 GeV mass range using pp collisions at $\sqrt{s} = 13$ TeV with the ATLAS detector*, [2407.07546](#).
- [90] R. Boughezal, F. Caola, K. Melnikov, F. Petriello and M. Schulze, *Higgs boson production in association with a jet at next-to-next-to-leading order*, *Phys. Rev. Lett.* **115** (2015) 082003 [[1504.07922](#)].
- [91] A. Atre, G. Azuelos, M. Carena, T. Han, E. Ozcan, J. Santiago et al., *Model-Independent Searches for New Quarks at the LHC*, *JHEP* **08** (2011) 080 [[1102.1987](#)].
- [92] D. Buttazzo, G. Degrassi, P.P. Giardino, G.F. Giudice, F. Sala, A. Salvio et al., *Investigating the near-criticality of the Higgs boson*, *JHEP* **12** (2013) 089 [[1307.3536](#)].
- [93] ATLAS collaboration, *Search for single production of vector-like T quarks decaying into Ht or Zt in pp collisions at $\sqrt{s} = 13$ TeV with the ATLAS detector*, *JHEP* **08** (2023) 153 [[2305.03401](#)].
- [94] CMS collaboration, *Search for pair production of vector-like quarks in leptonic final states in proton-proton collisions at $\sqrt{s} = 13$ TeV*, *JHEP* **07** (2023) 020 [[2209.07327](#)].
- [95] J.a.M. Alves, G.C. Branco, A.L. Cherchiglia, C.C. Nishi, J.T. Penedo, P.M.F. Pereira et al., *Vector-like singlet quarks: A roadmap*, *Phys. Rept.* **1057** (2024) 1 [[2304.10561](#)].
- [96] K.A. Beyer and S. Sarkar, *Ruling out light axions: The writing is on the wall*, *SciPost Phys.* **15** (2023) 003 [[2211.14635](#)].
- [97] M.D. Schwartz, *Quantum Field Theory and the Standard Model*, Cambridge University Press (2013).
- [98] A. Bilal, *Lectures on Anomalies*, [0802.0634](#).